Analog Applications Journal

Third Quarter, 2014

![Texas Instruments]

IMPORTANT NOTICE

Products		**Applications**	
Audio	www.ti.com/audio	Automotive and Transportation	www.ti.com/automotive
Amplifiers	amplifier.ti.com	Communications and Telecom	www.ti.com/communications
Data Converters	dataconverter.ti.com	Computers and Peripherals	www.ti.com/computers
DLP® Products	www.dlp.com	Consumer Electronics	www.ti.com/consumer-apps
DSP	dsp.ti.com	Energy and Lighting	www.ti.com/energy
Clocks and Timers	www.ti.com/clocks	Industrial	www.ti.com/industrial
Interface	interface.ti.com	Medical	www.ti.com/medical
Logic	logic.ti.com	Security	www.ti.com/security
Power Management	power.ti.com	Space, Avionics and Defense	www.ti.com/space-avionics-defense
Microcontrollers	microcontroller.ti.com	Video and Imaging	www.ti.com/video
RFID	www.ti-rfid.com		
OMAP™ Applications Processors	www.ti.com/omap	**TI E2E™ Community**	**e2e.ti.com**
Wireless Connectivity	www.ti.com/wirelessconnectivity		

Contents

Modern cars incorporate knock-sensor systems for engines to minimize knocking, which can maximize engine lifetime, increase power, and improve fuel efficiency. This article discusses engine knock basics and how to set up a knock-sensor signal-conditioning system.

Flat panel display link III, better known as FPD-Link III, is an interface used in many automotive applications to transport video and control signals from point to point. There are FPD-Link III serializers and deserializers (SerDes) that have been optimized either for the link between a processor and a display, or between the processor and a camera. This article provides an overview of these links, the advances that can be expected in the near future, and how to get even more out of the technology.

One common characteristic of the output of a sense-element is nonlinearity. Sensor nonlinearity leads to inaccuracies, or errors, in measurements. This article describes methods to correct the nonlinearity in the output of linear variable differential transformer (LVDT) position sensors that are used in many applications, including automotive hydraulic-valve position sensing.

Industrial and high-precision applications require strict control over non-deterministic noise. Some testing may be required to assure system quality because the typical noise value denotes the mean value of a parameter in a population of devices, and does not guarantee that individual devices will not exceed a certain level. Conventionally, testing devices can require tens or hundreds of seconds per device, vastly increasing time-to-market and production costs. This article uses existing theory and empirical data to explore test methodology for quickly testing for noise on any portion of the 1/f region. Also, theoretical and real-world results are compared using the OPA1652 low-noise audio op amp.

The single-end primary inductor converter (SEPIC), Zeta converter, and two-switch buck-boost converters have positive or non-inverting outputs. However, compared with a basic inverting buck-boost converter, all three non-inverting topologies have additional power components and reduced efficiency. This article presents operational principles, current stress and power-loss analysis of these buck-boost converters, and presents design criteria for an efficient non-inverting buck-boost converter.

For power supplies with an input power of 75 watts or greater, power factor correction (PFC) is required for many server, telecommunications and industrial applications. With the help of new semiconductor devices and new control methods, the modern PFC circuit has achieved very good performance at middle and heavy loads. However, during light-load conditions, the efficiency, THD and PF deteriorate significantly. This article provides a novel method to increase efficiency and reduce THD when the PFC enters the light-load condition.

To view past issues of the
Analog Applications Journal, **visit the Web site:**

www.ti.com/aaj

Subscribe to the AAJ:

www.ti.com/subscribe-aaj

Introduction

The *Analog Applications Journal* (AAJ) is a digest of technical analog articles published quarterly by Texas Instruments. Written with design engineers, engineering managers, system designers and technicians in mind, these "how-to" articles offer a basic understanding of how TI analog products can be used to solve various design issues and requirements. Readers will find tutorial information as well as practical engineering designs and detailed mathematical solutions as they relate to the following applications:

- Automotive
- Communications
- Enterprise Systems
- Industrial
- Personal Electronics

AAJ articles include many helpful hints and rules of thumb to guide readers who are new to engineering, or engineers who are just new to analog, as well as the advanced analog engineer. Where applicable, readers will also find software routines and program structures and learn about design tools. These forward-looking articles provide valuable insights into current and future product solutions. However, this long-running digest also gives readers archival access to many articles about legacy technologies and solutions that are the basis for today's products. This means the AAJ can be a relevant research tool for a very wide range of analog products, applications and design tools.

How to set-up a knock-sensor signal-conditioning system

By Yvette Tran
Automotive System Applications Engineer

Introduction

Engine knock occurs in engine cylinders because of improper ignition timing or faulty components. Modern cars incorporate knock-sensor systems for engines to minimize knocking, which can maximize engine lifetime, increase power, and improve fuel efficiency. This article discusses engine knock basics and how to set up a knock-sensor signal-conditioning system.

Basics of engine knock

Engine knock, or detonation, is uncontrolled ignition of pockets of air and fuel mixture in a cylinder in addition to the pocket initiated by the spark plug. Engine knock can greatly increase cylinder pressure, damage engine components, and cause a pinging sound.

In normal combustion, an internal-combustion engine burns the air and fuel mixture in a controlled fashion. Combustion should start a few crankshaft degrees prior to the piston passing the top dead center. This timing advance is necessary because it takes time for the air and fuel mixture to fully burn and it varies with engine speed and load. If timed correctly, maximum cylinder pressure occurs a few crankshaft degrees after the piston passes the top dead center. The completely ignited air and fuel mixture then pushes the piston down with the greatest force, resulting in the maximum torque applied to the crankshaft for each cycle.

Today's engines are designed to minimize emissions and maximize power as well as fuel economy. This can be achieved by optimizing the ignition spark timing to maximize the torque. With this timing control, the spark plug ignites the air and fuel mixture from the ignition point to the cylinder walls and burns it smoothly at a particular rate. Deviations from normal combustion, such as igniting too soon, can cause engine knock and, in extreme cases, result in permanent engine damage. Other causes of engine knock include using the wrong octane gasoline or defective ignition components.

Signal-conditioner interface

Modern cars have a knock-sensor system to detect engine knock for each cylinder during a specified time after top dead center called the knock window. A typical system consists of a piezoelectric sense element and signal conditioner. The sensor detects vibrations and the signal conditioner processes the signal and sends a voltage signal to the engine control module. The module interprets the knock signal to control timing and improve engine efficiency. Knock sensors typically are mounted on the engine block (Figure 1).

Figure 1. Knock sensor mounted to an engine block
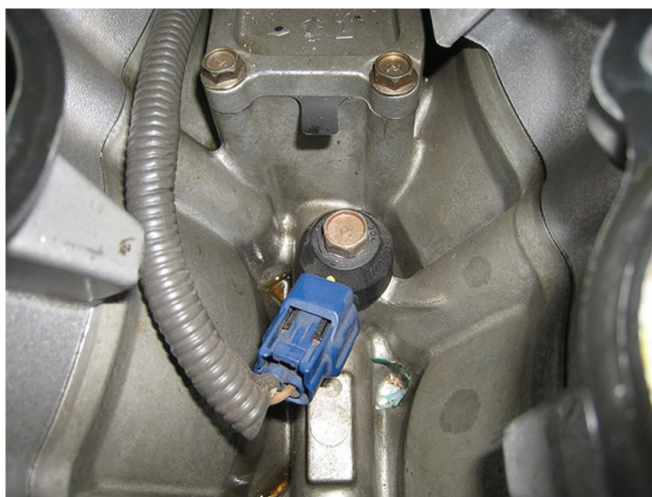
Figure 2. TPIC8101 block diagram with coefficients
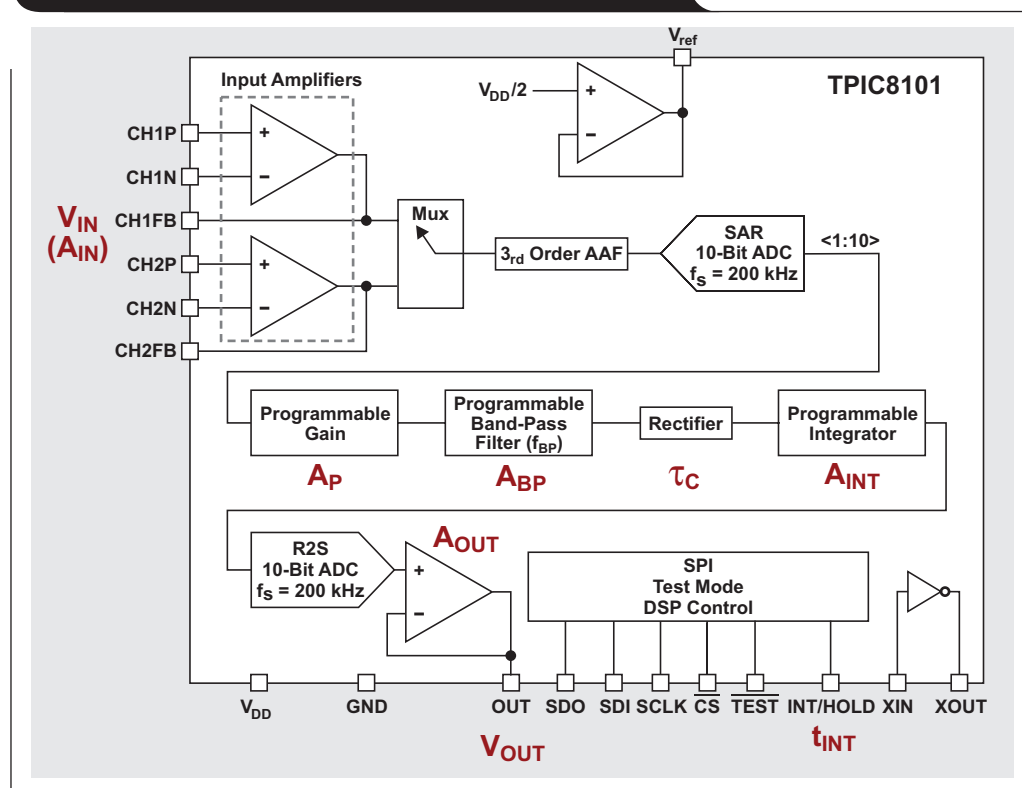
Coefficient descriptions:

V_{IN} = Amplitude of input voltage peak

V_{OUT} = Output voltage

A_{IN} = Input amplifier gain setting

A_P = Programmable gain setting

A_{BP} = Gain of bandpass filter

A_{INT} = Gain of integrator

t_{INT} = Integration time from 0.5 ms to 10 ms

A_{OUT} = Output buffer gain

τ_C = Programmable integrator time constant

V_{RESET} = Reset voltage from which the integration operation starts

The simplified diagram in Figure 2 shows the TPIC8101 dual-channel, highly-integrated, signal-conditioner interface from Texas Instruments that can be connected between the knock-sensing element and engine control module. The two internal wide-band amplifiers (Figure 3) provide interface to the piezoelectric sensors. The outputs of the amplifiers feed a channel-select mux switch (Figure 2), followed by a third-order anti-aliasing filter (AAF). The signal is then converted using an analog-to-digital converter (ADC) prior to the programmable gain stage. The gain stage feeds the signal to a programmable bandpass filter to process the particular frequency component associated with the engine and knock sensor. The output of the bandpass filter is full-wave rectified and then integrated based on a programmed time constant and integration time period. At the start of each knock window, the integrator output is reset. The integrated signal is converted to an analog format with a digital-to-analog (DAC), but can be connected directly to a microprocessor. The processor reads the data and adjusts the spark-ignition timing to reduce knock while optimizing fuel efficiency relative to load and engine RPM.

Figure 3. Detail of interface to input amplifiers

A_{IN} = 1 is the TP1C8101 default setting
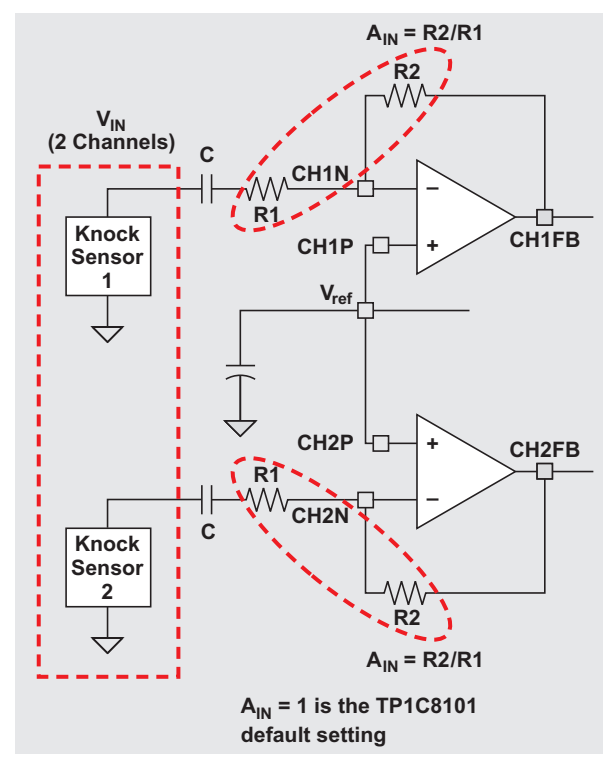
Internal blocks

The operation of the signal-conditioner interface is defined by its transfer function:

$$V_{OUT} = V_{IN} \times A_P \times \frac{8}{\pi} \times \frac{t_{INT}}{\tau_C} + 0.125 \qquad (1)$$

This equation is based off of the internal blocks of the signal conditioner. The equation's component values are then programmed into the device by the graphical user interface (GUI) through a serial peripheral interface (SPI) port.

Derivation of transfer function

The following steps outline how Equation 1 was derived from the functional blocks in Figure 2.

To begin derivation, the output voltage is defined as:

$$V_{OUT} = V_{IN} \times A_{IN} \times A_P \times A_{BP} \times A_{INT} \times \frac{t_{INT}}{\tau_C} \times A_{OUT} + V_{RESET} \qquad (2)$$

Let the amplitude of V_{IN} be equal to:

$$V_{IN} = \sin(A \times t) \times V_{IN} \qquad (3)$$

Also, let: $t_{INT} = \dfrac{N}{f_{BP}}$ and $B = \dfrac{\pi}{A}$, $\qquad (4)$

where f_{BP} is the filter center frequency and N is the number of cycles.

Therefore, $A = \pi \times f_{BP}$ and $B = \dfrac{1}{f_{BP}}$. $\qquad (5)$

The integrator operation is performed N times from 0 to B. This will cover the positive side of the input. Full-wave rectification is compensated later through the other gain coefficients. Substitute V_{IN} and integrate from 0 to $1/f_{BP}$.

$$V_{OUT} = N \times \int_0^{1/f_{BP}} V_{IN} \times \sin(\pi \times f_{BP} \times t) dt \times A_{IN} \times A_P \times A_{BP} \times A_{INT} \times \frac{1}{\tau_C} \times A_{OUT} + V_{RESET} \qquad (6)$$

$$V_{OUT} = N \times \frac{1}{\pi \times f_{BP}} \times V_{IN} \times \left[-\cos(\pi \times f_{BP} \times t)_0^{1/f_{BP}} \right] dt \times A_{IN} \times A_P \times A_{BP} \times A_{INT} \times \frac{1}{\tau_C} \times A_{OUT} + V_{RESET} \qquad (7)$$

Substitute for N:

$$V_{OUT} = (t_{INT} \times f_{BP}) \times \frac{1}{\pi \times f_{BP}} \times V_{IN} \times \left[-\cos(\pi) + 1 \right] dt \times A_{IN} \times A_P \times A_{BP} \times A_{INT} \times \frac{1}{\tau_C} \times A_{OUT} + V_{RESET} \qquad (8)$$

$$V_{OUT} = \frac{t_{INT} \times V_{IN}}{\pi} \times [1+1] dt \times A_{IN} \times A_P \times A_{BP} \times A_{INT} \times \frac{1}{\tau_C} \times A_{OUT} + V_{RESET} \qquad (9)$$

$$V_{OUT} = \frac{V_{IN}}{\pi} \times 2 \times A_{IN} \times A_P \times A_{BP} \times A_{INT} \times \frac{t_{INT}}{\tau_C} \times A_{OUT} + V_{RESET} \qquad (10)$$

Let $A_{INT} = 2$, $A_{IN} = A_{OUT} = 1$, $V_{RESET} = 0.125$, and

$$A_{BP} = \frac{2 \times \dfrac{\omega_c \times \omega}{Q_{BP}}}{\sqrt{\left(\omega_C^2 - \omega^2\right)^2 + \left(\omega_C \times \dfrac{\omega}{Q_{BP}}\right)^2}}, \qquad (11)$$

where Q_{BP} is a Q factor that characterizes a resonator's bandwidth relative to its center frequency.

Evaluate at the center frequency, $\omega = \omega_C$. Therefore, $A_{BP} = 2$. Plug in all values for A_{INT}, A_{IN}, A_{OUT}, A_{BP}, V_{RESET} to get:

$$V_{OUT} = \frac{V_{IN}}{\pi} \times 2 \times A_P \times 2 \times 2 \times \frac{t_{INT}}{\tau_C} + 0.125, \qquad (12)$$

where V_{IN} is entered as a peak value.

Therefore, the final solution is Equation 1:

$$V_{OUT} = V_{IN} \times A_P \times \frac{8}{\pi} \times \frac{t_{INT}}{\tau_C} + 0.125$$

Application example

Next are the steps necessary to set up the signal conditioner.

Requirements

The required known values are V_{IN}, oscillation frequency, t_{INT}, and V_{OUT}. For this example, the know values are:

- V_{IN} = 7.3 kHz, 300 mV$_{PP}$ (knock sensor specification)
- Oscillator = 6 MHz (microprocessor clock specification)
- Knock window (t_{INT})= 3 ms (system specification)
- V_{OUT} = 4.5 V (microprocessor interface specification)

Calculating remaining coefficients

Now that A_{INT}, A_{OUT}, A_{BP}, V_{RESET} are set, the remaining coefficients need to be calculated:

- Programmable gain (A_P)
- Integration time constant (τ_C)
- Input amplifier gain (A_{IN}): Set A_{IN} = 1

$$\tau_C = \frac{t_{INT}}{2 \times \pi \times V_{OUT}} = \frac{3 \text{ ms}}{2 \times \pi \times 4.5 \text{ V}} = 106 \text{ µs} \qquad (13)$$

With known values, Equation 1 can now be solved for A_P:

$$4.5 \text{ V} = 150 \text{ mV} \times A_P \times \frac{8}{\pi} \times \frac{3 \text{ ms}}{100 \text{ µs}} + 0.125 \rightarrow A_P = 0.38 \qquad (14)$$

Note that the 100-µs value for τ_C reflects a minor adjustment required to program the value as indicated in the following discussion.

How to program coefficients

After the coefficients have been calculated, they need to be entered into the GUI. The following paragraph is an overview of the data values that would be entered with the GUI software for the TIDA-00152 reference design (See Reference 1).

For f_C, Table 1 show that the closest bandpass frequency to 7.3 kHz is 7.27 kHz, which corresponds to a decimal value of 42 and a hex value of 2A. For A_P, the closest value to 0.38 in Table 1 is 0.381, which corresponds to a decimal value of 34 and a hex value of 22. For τ_C, the closest value to 106 µs in Table 1 is 100 µs, which corresponds to a decimal value of 10 and a hex value of 0A.

Table 1. Part of SPI look up table from page 10 in the TPIC8101 datasheet

| | τ_C | | | A_P | | A_P |
DECIMAL VALUE (D4…D0)	INTEGRATOR TIME CONSTANT (µSEC)	BAND-PASS FREQUENCY (kHz)	GAIN	DECIMAL VALUE (D5…D0)	BAND-PASS FREQUENCY (kHz)	GAIN
0	40	1.22	2	32	4.95	0.421
1	45	1.26	1.882	33	5.12	0.4
2	50	1.31	1.778	34	5.29	0.381
3	55	1.35	1.684	35	5.48	0.364
4	60	1.4	1.6	36	5.68	0.348
5	65	1.45	1.523	37	5.9	0.333
6	70	1.51	1.455	38	6.12	0.32
7	75	1.57	1.391	39	6.37	0.308
8	80	1.63	1.333	40	6.64	0.296
9	90	1.71	1.28	41	6.94	0.286
10	100	1.78	1.231	42	7.27	0.276
11	110	1.87	1.185	43	7.63	0.267
12	120	1.96	1.143	44	8.02	0.258

Figure 4. GUI values
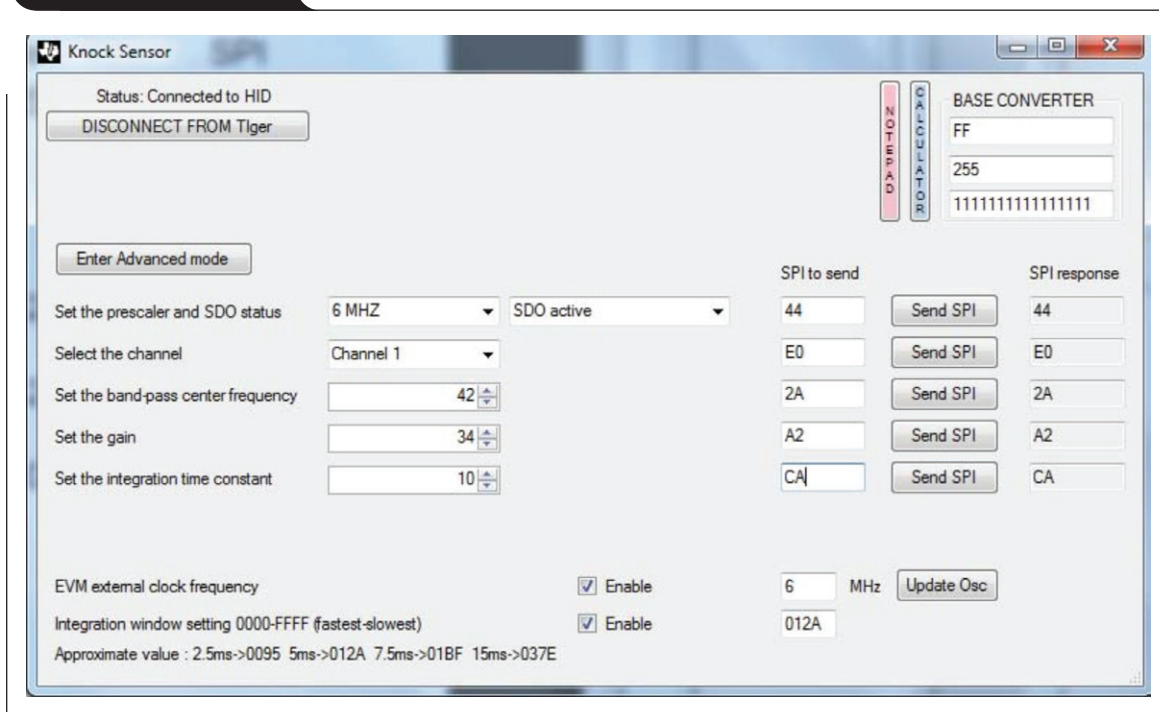
Enter in 6 MHz for the oscillator frequency and 1 for the number of channels. GUI values should look like those in Figure 4.

Following the previous steps should result in the waveform in Figure 5. For more waveforms with different degrees of amplitude modulation, see the TIDA-00152 reference design test data in Reference 1.

Conclusion

Engine knock control is necessary for optimal engine performance and for protecting the engine. The dual-channel input and advanced signal conditioning of the TPIC8101 knock-sensor interface reduces the processing load on the engine control module.

References

1. TIDA-00152 reference design for Automotive Acoustic Knock-Sensor Interface. Includes links to schematic/block diagram, test data, design files, and bill of materials. Available: **www.ti.com/3q14-tida00152**

Related Web sites

TPIC8101 product folder:
www.ti.com/3q14-tpic8101

TPIC8101 EVM User's Guide:
www.ti.com/3q14-tidu287

TPIC8101 Datasheet:
www.ti.com/3q14-SLIS110

Subscribe to the AAJ:
www.ti.com/subscribe-aaj

Figure 5. Example waveform

V_{IN} = 300 mV$_{pp}$, 7270 kHz (200 mV/div)

INT, 3 ms (5 V/div)

— 4.48 V

Output (2 V/div)

Time (1 ms/div)
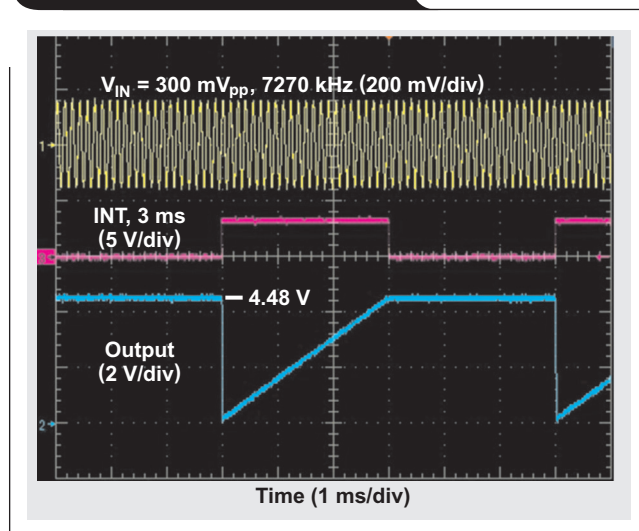
FPD-Link III – doing more with less

By Mark Sauerwald
Applications Engineer, Automotive Connectivity and Ethernet

Flat panel display link III, better known as FPD-Link III, is an interface used in many automotive applications to transport video from point to point. This interface enables the transport of high-definition digital video, as well as a bidirectional control channel, over a low-cost cable, either twisted pair or coax. There are FPD-Link III serializers and deserializers (SerDes) that have been optimized either for the link between a processor and a display, or between the processor and a camera (Figure 1). This article provides an overview of these links, the advances that can be expected in the near future, and how to get even more out of the technology.

Not long ago, cameras were a novel feature in an automobile, mostly used in larger vehicles to aid in seeing behind the vehicle while backing up. Today, backup cameras are included even in low-cost, sub-compact cars. As automobiles develop, there will be more and more applications for cameras in the vehicle, and the cameras will become more and more sophisticated.

The backup camera allows the driver to see directly behind the vehicle, something that is difficult if not impossible to do with mirrors alone. The next step beyond this is surround-view systems. In a typical surround-view system, there are four cameras mounted on the car – usually one in each of the front and rear bumpers, and one in each side view "wing mirror." Each camera is fitted with a fisheye lens, so that between the four images, a complete image of what is happening around the car can be generated. In a surround-view system, the four fisheye images

are presented to a video image processor such as the TI DRA74x "Jacinto 6." This processor removes the fisheye distortion, changes the apparent point of view, and merges the four images together to generate a virtual bird's-eye view of the automobile, allowing the driver to clearly see any obstacles in front, behind, or to either side of the vehicle.

When these images are processed, certain portions of the image are magnified, while others are compressed. In order to retain high image quality, the density of pixels needs to be higher than what a standard human viewer would require. The current automotive imagers support 1-megapixel (MP) images, but 2-MP imagers are on the horizon. To support this next generation of image sensors, automotive designers can expect to see new SerDes designs optimized for 2-MP imagers. Along with the higher data rates that these imagers require, there will be next-generation interfaces to be supported.

Another aspect of the evolution of automotive vision systems is that the industry is moving from the single camera system, such as a backup camera, to where multiple cameras are being used. With multiple cameras, imager synchronization becomes an important feature. In an application such as the surround view application, having all of the imagers synchronized makes the processing easier. However, if two cameras are to be used in tandem to create a stereo image of a 3D scene in front of the vehicle, synchronization is required to determine the accurate position of a moving object – or even a stationary object as

Figure 1. Typical interface with FPD-Link III
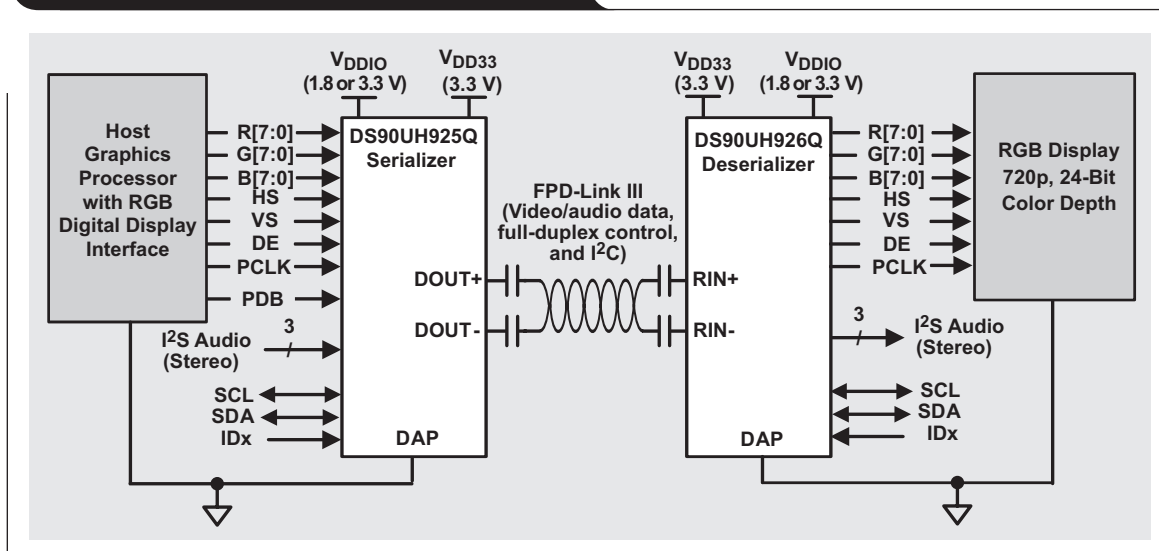
seen from a moving vehicle. Next-generation systems will have to accommodate the potential for supporting multiple cameras that are all synchronized.

In many areas, adding more capabilities to an existing technology has made the interconnects more complicated and more expensive. For example, adding copy protection to the link from your home DVD player to your video monitor requires changing from an analog coax cable to an HDMI cable. The new connection method gives better quality video, along with the copy protection. But this is at the cost of a much more expensive cable/connector ecosystem, and there's also the difficulty of supporting longer cable runs.

When confronted with a similar issue within the automobile, FPD-Link III was extended to allow the same twisted-pair cable to carry copy-protected content from a Blu-ray™ player or server to a back-seat entertainment screen. The specification is to do so with no penalty for the cost of the media, or the range of the older, non-copy-protected media. The chipset shown in Figure 1 embodies this technology. In these devices, the same information that was carried over separate conductors is now encoded and carried along the FPD-Link III – sharing the same conductors that carry the video content.

Getting video out of a camera and to the processor, or from a Blu-ray player to a screen, is not enough. In both cases, control signals going in the opposite direction are also required. In the case of the camera, the processor needs to configure the imager. In the case of the back-seat entertainment panel, the user interface is often a touch screen, and touch commands must be sent back from the screen to the processor.

FPD-Link III handles this with an integrated back channel, which allows the same piece of coax or twisted pair to carry video in one direction, and to have an independent, bidirectional control channel sharing the same conductor. This allows the cable to remain thin, flexible

and inexpensive. But what about power – cameras and displays still need to be powered. Can the same cable be used to power the device as well as provide a communications link?

Power over coax

The key to using the same cable for power and communications is to think of what is going on in the frequency domain. The video forward channel and the bidirectional control channel on FPD-Link III are able to share the same cable because they occupy different spaces in the frequency domain. Using the DS90UB913A-Q1 and DS90UB914A-Q1 as an example, the control channel occupies the space from about 1 MHz to about 5 MHz. The video channel occupies a space from about 70 MHz to about 700 MHz. The addition of power to the same cable must be accomplished without interfering with either of these two bands.

For power over coax (POC), a circuit is required that will split the input signal into two branches (Figure 2). One branch carries DC power for the POC circuit, and the second branch carries the signals without DC power. To do this, an element is placed in the signal-path branch that passes both the back channel and the forward channel, but blocks the DC. A simple capacitor works for this. The 0.1-µF capacitor has very low impedance from the start of the 1-MHz back-channel band through the 700-MHz upper limit. It is readily available and inexpensive. Parasitic inductance for a 0.1-µF, 0603 capacitor is on the order of 1 nH, so it does not really come into play within the band of interest. The capacitors are a good choice to separate the AC signals from the DC power.

The other branch, one that passes the DC but doesn't interfere with the AC signal, is a bit harder. Since the data channels are being passed over a controlled impedance transmission line, the impedance of the low-pass circuit must be large over the band of the forward channel.

Figure 2. Block diagram showing the power-over-coax topology
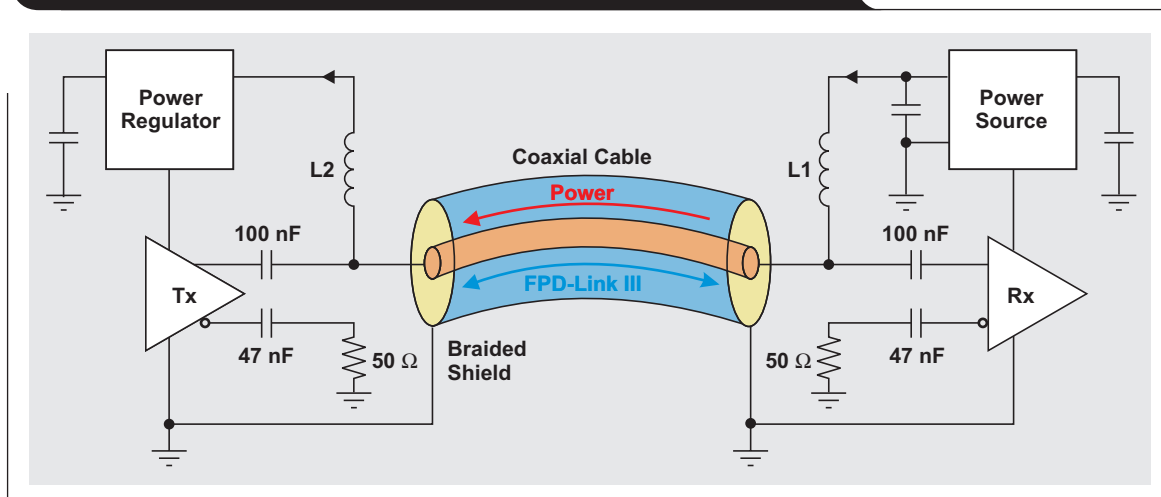
Figure 3. Impedance plots of various inductors
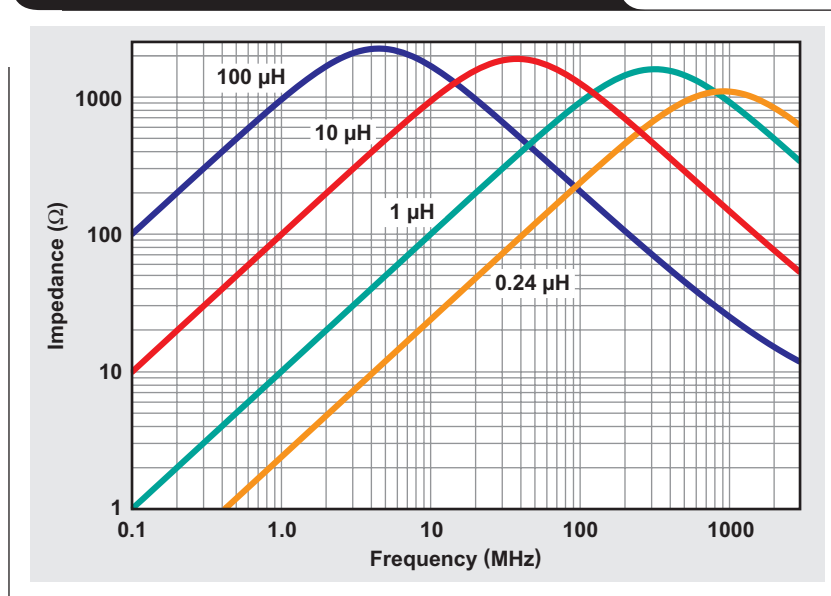
For the power circuit to not interfere with the data path, the impedance of this circuit must be greater than about 20 times the characteristic cable impedance. So for a 50-Ω coax line, the impedance should be greater than 1 kΩ from 1 MHz up to 700 MHz. An ideal inductor would work for this application.

Unfortunately, ideal inductors are much harder to find than ideal capacitors. To have over 1-kΩ impedance at the 1-MHz lower band of the back channel, a 100-µH inductor is required. But a typical 100-µH inductor has a parasitic capacitance, which drops its impedance below 1 kΩ at frequencies above 70 MHz. Thus, it would interfere with the forward channel.

Figure 3 shows plots of the impedance of some different inductors versus frequency. Notice how impedance rises up to a certain point where the parasitic capacitance becomes dominant, and then the impedance drops. This figure shows that a 100-µH inductor will do a good job of blocking the control channel since its impedance is about 1 kΩ from 1 MHz up through 5 MHz. However, when the forward channel is at 150 MHz, the impedance drops to about 200 Ω. The solution is to use a circuit with two series inductors, a 100-µH inductor to block the control channel, and a second, smaller inductor that blocks the video channel. It turns out that about 5 µH is right for the second inductor.

The physics of the requirements dictate the values of the inductors (100 µH and 4.7 µH), but the physical size is dominated by the ability of the core to sustain the magnetic field. Physically, smaller inductors have lower saturation currents. One way to use a smaller inductor is to reduce the current requirement of the circuit. This can be done by increasing the voltage that is being carried by the coax cable. If the camera requires 1.5 W, and power over the coax is a voltage of 5 V, then the current required is 300 mA. The 100-µH inductor that was chosen is probably about the smallest physical size that could be tolerated (it is 7 mm x 7 mm x 4 mm in size). However, if a 12-V supply is used, then only 125 mA is required. An inductor that supports this lower current occupies about one-fourth of the physical space of one that will support the 300 mA.

Conclusion

Video is becoming a bigger part of the modern automobile. FPD-Link III is an ideal technology to support today's and tomorrow's needs, minimizing the system cost through using inexpensive cable to do more. It is also a technology that is ready to keep pace with future advances.

Related Web sites

For more information about FPD-Link III solutions, visit:
www.ti.com/3q14-fpd

www.ti.com/3q14-DS90UH925QQ1

www.ti.com/3q14-DS90UH926QQ1

www.ti.com/3q14-DS90UB913AQ1

www.ti.com/3q14-DS90UB914AQ1

Subscribe to the AAJ:
www.ti.com/subscribe-aaj

Dealing with nonlinearity in LVDT position sensors

By Arun T Vemuri
Systems Architect, Enhanced Industrial

Introduction

Sense elements convert a physical quantity of interest into electrical signals. One common characteristic of the output of a sense-element is nonlinearity – the output of the a sense element does not vary linearly with the physical quantity of interest. This nonlinearity leads to inaccuracies, or errors, in measurements.

This article describes methods to correct the nonlinearity in the output of linear variable differential transformer (LVDT) position sensors that are used in many applications, including automotive hydraulic-valve position sensing. This discussion also applies to other types of automotive sensor applications such as ultrasonic park-assist.

Sensors with high-frequency outputs

The electrical signal produced by many sense elements is a relatively high-frequency signal. This is either because the stimulus to the sense element is a high-frequency signal, or the physical quantity being measured is high frequency in nature. For example, position measurement of automotive hydraulic valves using LVDT position sensors. This sensor is high frequency because the LVDT primary coil is excited using a high-frequency signal – say, 5 kHz. Similarly, the output of piezoelectric transducers used in ultrasonic park-assist applications is high frequency because the transducers measure the intensity of ultrasonic waves, whose signal frequency is greater than 20 kHz.

In such high-frequency-sensor signal outputs, the signal information is most often embedded in the amplitude of the signal. Figure 1 shows a time-plot of a sensor signal which is high frequency, and the amplitude represents the variation of the physical quantity that the sensor is measuring. The mathematical representation of such a signal is:

$$y(t) = A_C \sin(\omega_C t) + A_S \sin(\omega_S t) A_C \sin(\omega_C t), \qquad (1)$$

where A_C is the amplitude of the sensor excitation, ω_C is the sensor-excitation frequency in rads/s, A_S is the amplitude of the physical quantity of interest, and ω_S is the frequency of the physical quantity of interest in rads/s.

It is assumed that the amplitude of the signal of interest is less than the amplitude of the high-frequency carrier signal so that y(t) is an undistorted amplitude-modulated signal.

Note that in some cases, the signal information could be embedded in the signal's frequency. For example, if an ultrasonic transducer in the bumper or wing mirror of a moving automobile is used to measure distance to another moving vehicle, then the frequency of the signal will have information about the relative speeds of the vehicle based on the Doppler effect.

In this article, the focus is on extracting the amplitude information from the output of the high-frequency sensor. The technique of extracting amplitude information is called amplitude demodulation.

Amplitude-demodulation techniques have been in existence ever since AM radio transmissions began in the early 1900s. Many solutions have been implemented in both the analog and digital domain to extract the amplitude information from a signal. Further, the demodulation processes could extract just the amplitude of the signal, or could also extract the phase of the sensor output signal relative to the sensor stimulus. The former demodulation technique is called asynchronous demodulation while the latter technique is called synchronous demodulation.

Based on the above definitions, the focus of this article is limited to one specific family of amplitude-extraction techniques – digital asynchronous amplitude demodulation.

Figure 1. High-frequency sensor output with signal information in the amplitude
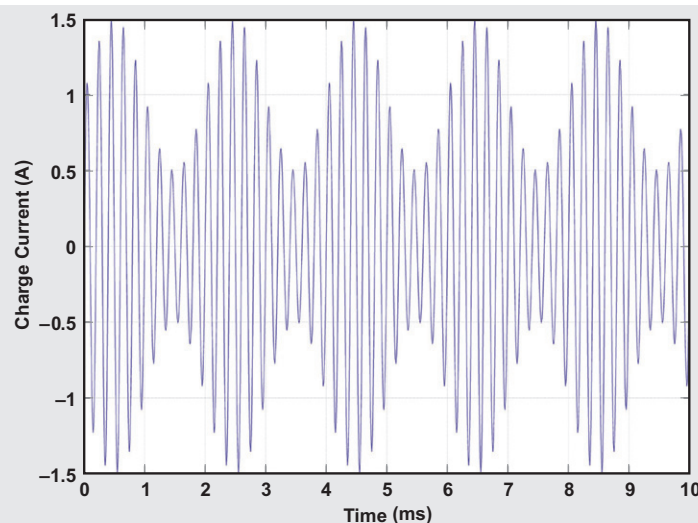
Why is this narrow family of techniques important? With the advent of advanced manufacturing techniques for mixed-signal integrated circuits (ICs), such as the LBC8LV process at Texas Instruments, mixed-signal signal conditioners are available to support a variety of sensors. With such sensors, signal conditioning occurs partly in the analog domain and partly in the digital domain. Even though signal-conditioning architectures have quantization aspects, such devices offer flexibility and, if designed right, offer sufficient accuracy for most sensor applications. Application engineers can easily customize signal conditioners for their specific application scenario and speed up their product-development cycles.

The PGA450-Q1 from Texas Instruments is an example of a mixed-signal signal conditioner for automotive sensors used in ultrasonic park-assist applications. This signal conditioner specifically amplifies the electrical signal using an amplifier and extracts the amplitude of the signal using the digital asynchronous, amplitude-demodulation technique.

Digital asynchronous, amplitude-demodulation techniques

Two methods of the digital asynchronous, amplitude-demodulation technique are investigated: peak and average.

Peak Method

In this method of asynchronous demodulation, the peak value of the sensor output signal in every frequency cycle

is extracted. That is, this process discretizes the signal in time at a frequency of the underlying carrier signal.

If the frequency of the underlying signal is known (which is usually the case), and if the signal is sinusoidal (which is a typical high-frequency excitation signal), then the extracted peak value is the amplitude of the sine wave in each cycle. That is, the peak value in the nth carrier-frequency cycle can be mathematically expressed:

$$y_P\left(t = nT_c\right) = A_C + A_S\sin\left[\omega_S\left(n - \frac{3}{4}\right)T_C\right], \tag{2}$$

where $T_C = 2\pi/\omega_C$.

The PGA450-Q1 implements the peak method of demodulation.

Average Method

In this method of asynchronous demodulation, the sensor signal is first rectified. The rectified output is then filtered using a low-pass filter. Mathematically, the full-wave rectified output of the signal described in Equation 1 is:

$$\begin{aligned} y_R(t) &= \left|y\left(t\right)\right| \\ &= \left[A_C\sin\left(\omega_Ct\right) + A_S\sin\left(\omega_St\right)A_C\sin\left(\omega_Ct\right)\right]u(t), \end{aligned} \tag{3}$$

where $u(t)$ is a square wave with amplitude equal to 1 and frequency equal to ω_C.

Using Fourier series, the square wave can be written as:

$$u\left(t\right) = \frac{4}{\pi}\sum_{n=0}^{\infty}\frac{\sin\left[\left(2n+1\right)\omega_Ct\right]}{2n+1} \tag{4}$$

Therefore, the rectified output can be written as:

$$y_R(t) = \left[A_C\sin\left(\omega_Ct\right) + A_S\sin\left(\omega_St\right)A_C\sin\left(\omega_Ct\right)\right]\left\{\frac{4}{\pi}\sum_{n=0}^{\infty}\frac{\sin\left[\left(2n+1\right)\omega_Ct\right]}{2n+1}\right\} \tag{5a}$$

$$y_R(t) = \frac{4A_C}{\pi}\sum_{n=0}^{\infty}\frac{\sin\left(\omega_Ct\right)\sin\left[\left(2n+1\right)\omega_Ct\right]}{2n+1} + \left\{\frac{4A_SA_C}{\pi}\sum_{n=0}^{\infty}\frac{\sin\left(\omega_St\right)\sin\left(\omega_Ct\right)\sin\left[\left(2n+1\right)\omega_Ct\right]}{2n+1}\right\} \tag{5b}$$

$$\begin{aligned} y_R(t) &= \frac{4A_C}{\pi}\sin^2\left(\omega_Ct\right) + \frac{4A_SA_C}{\pi}\sin\left(\omega_St\right)\sin^2\left(\omega_Ct\right) + \frac{4A_C}{\pi}\sum_{n=1}^{\infty}\frac{\sin\left(\omega_Ct\right)\sin\left[\left(2n+1\right)\omega_Ct\right]}{2n+1} \\ &\quad + \left\{\frac{4A_SA_C}{\pi}\sum_{n=1}^{\infty}\frac{\sin\left(\omega_St\right)\sin\left(\omega_Ct\right)\sin\left[\left(2n+1\right)\omega_Ct\right]}{2n+1}\right\} \end{aligned} \tag{5c}$$

$$\begin{aligned} y_R(t) &= \frac{2A_C}{\pi} - \frac{2A_C}{\pi}\cos\left(2\omega_Ct\right) + \frac{2A_SA_C}{\pi}\sin\left(\omega_St\right) - \frac{2A_SA_C}{\pi}\sin\left(\omega_St\right)\cos\left(2\omega_Ct\right) \\ &\quad + \frac{4A_C}{\pi}\sum_{n=1}^{\infty}\frac{\sin\left(\omega_Ct\right)\sin\left[\left(2n+1\right)\omega_Ct\right]}{2n+1} + \left\{\frac{4A_SA_C}{\pi}\sum_{n=1}^{\infty}\frac{\sin\left(\omega_St\right)\sin\left(\omega_Ct\right)\sin\left[\left(2n+1\right)\omega_Ct\right]}{2n+1}\right\} \end{aligned} \tag{5d}$$

Filtering the rectified output using a low-pass filter with a gain of 0 dB and the cutoff frequency is ω_C, the filtered output can be expressed:

$$y_{LPF}(t) = LPF\left[y_R(t)\right] \cong \frac{2A_C}{\pi} + \frac{2A_S A_C}{\pi}\sin(\omega_S t) \qquad (6)$$

Equation 6 shows that the signal can be extracted using this method.

Effect of nonlinearity

In a linear system, the output of the system is proportional to its input; in other words, the output is:

$$y = \sum_{i=1}^{1} a_i x^i, \qquad (7)$$

where x is the input to the system, y is the output of the system, and a_i is the coefficient. For simplicity of analysis, the offset term (the term that is independent of the input signal) has been neglected.

In a nonlinear system, the output of the system has higher-order input terms; or the output is:

$$y = \sum_{i=1}^{\infty} a_i x^i. \qquad (8)$$

In the context of LVDT signal conditioning, the amplitude modulated signal given in Equation 1 could be affected by nonlinearity. The possible causes of nonlinearity are:

1. Distorted drive signal, or the carrier has higher-order harmonics. The carrier could have high-order harmonics because the carrier signal itself is the output of a nonlinear system:

$$y_C = \sum_{i=1}^{\infty} a_i \left[A_C \sin(\omega_C t)\right]^i$$

2. The nonlinear signal chain, or the signal output, is nonlinear with regards to its input:

$$y_S = \sum_{i=1}^{\infty} a_i \left[A_C \sin(\omega_C t) + A_S \sin(\omega_S t) A_C \sin(\omega_C t)\right]^i$$

3. Nonlinear transducer, or the transducer output, is nonlinear with regards to the physical quantity it is measuring:

$$y_S = \sum_{i=1}^{\infty} a_i \left[A_S \sin(\omega_S t)\right]^i$$

Note that the first two sources of the nonlinearities are a result of a non-ideal signal generator/conditioner, while the third source of nonlinearity is from the transducer.

Also, all nonlinearities can be present in the system at the same time, making the output of the signal chain a complex mathematical expression.

Dealing with nonlinearity

The two sources of nonlinearity that are a result of non-ideal signal generator and conditioner will now be addressed. Also, a second-order nonlinear system, which is one of the common forms of nonlinear systems, will be analyzed. This analysis can be extended to higher-order nonlinearities as well as a nonlinear transducer output.

Distorted drive signal

In the presence of a distorted drive signal (or carrier signal), the amplitude-modulated carrier signal given in Equation 1 can be written as Equation 9 by setting $a_1 = 1$ and $a_2 = b$ after trigonometric manipulations.

$$
\begin{aligned}
y(t) &= A_C \sin(\omega_C t) + A_S \sin(\omega_S t) A_C \sin(\omega_C t) \\
&\quad + b\left[A_C \sin(\omega_C t)\right]^2 + bA_S \sin(\omega_S t)\left[A_C \sin(\omega_C t)\right]^2
\end{aligned} \qquad (9a)
$$

$$
\begin{aligned}
y(t) &= A_C \sin(\omega_C t) + A_S \sin(\omega_S t) A_C \sin(\omega_C t) \\
&\quad + bA_C^2\left[1 - \sin(2\omega_C t)\right] + bA_S A_C^2 \sin(\omega_S t)\left[1 - \sin(2\omega_C t)\right]
\end{aligned} \qquad (9b)
$$

Equation 9 shows that the output of the transducer has frequency components at 0 rad/s and at around $2\omega_C$, in addition to a signal around ω_C

One clear way to minimize the frequency components at 0 rad/s and at around $2\omega_C$ is to use a bandpass filter with the center frequency set at ω_C and with sufficient bandwidth. The bandwidth specifically should be such that there is no significant attenuation at $\omega_C \pm \omega_S$. With such a bandpass filter, the output of the bandpass filter is:

$$
\begin{aligned}
y_{BPF}(t) &= BPF\left[y(t)\right] \\
&\cong A_C \sin(\omega_C t) + A_S \sin(\omega_S t) A_C \sin(\omega_C t)
\end{aligned} \qquad (10)
$$

This bandpass filter output can then be demodulated either by using the peak or average method to extract the transducer signal.

Nonlinear signal chain

The presence of second-order signal-chain nonlinearity causes the amplitude modulated signal to be modified to be:

$$y(t) = \sum_{i=1}^{2} a_i \left[A_C \sin(\omega_C t) + A_S \sin(\omega_S t) A_C \sin(\omega_C t)\right]^i \qquad (11)$$

Setting a1 = 1 and a2 = b, and following trigonometric manipulation, Equation 11 can be written:

$$y(t) = \left\{ \left[A_C \sin(\omega_C t) + A_S \sin(\omega_S t) A_C \sin(\omega_C t) \right] + b \left[A_C \sin(\omega_C t) \right]^2 \right\}$$

$$+ b \left\{ \left[A_S \sin(\omega_S t) A_C \sin(\omega_C t) \right]^2 \right\} + b \left[2 A_C \sin(\omega_C t) A_S \sin(\omega_S t) A_C \sin(\omega_C t) \right] \tag{12a}$$

$$y(t) = \left[A_C \sin(\omega_C t) + A_S \sin(\omega_S t) A_C \sin(\omega_C t) \right] + b A_C^2 \left[1 - \sin(2\omega_C t) \right]$$

$$+ b A_C^2 A_S^2 \left[1 - \sin(2\omega_C t) \right] \left[1 - \sin(2\omega_S t) \right] + 2 b A_C^2 A_S \left[1 - \sin(2\omega_C t) \right] \sin(\omega_S t) \tag{12b}$$

$$y(t) = \left[A_C \sin(\omega_C t) + A_S \sin(\omega_S t) A_C \sin(\omega_C t) \right] + b A_C^2 \left[1 - \sin(2\omega_C t) \right]$$

$$+ b A_C^2 A_S^2 \left[1 - \sin(2\omega_C t) - \sin(2\omega_S t) + \sin(2\omega_C t) \sin(2\omega_S t) \right] + 2 b A_C^2 A_S \left[\sin(\omega_S t) - \sin(2\omega_C t) \sin(\omega_S t) \right] \tag{12c}$$

Equation 12, once again, shows that the output of the transducer has frequency components at 0 rad/s and at around $2\omega_C$ and higher frequencies, in addition to the signal around ω_C

Again, using a bandpass filter with the center frequency set at ω_C, and with sufficient bandwidth, the nonlinearity-induced frequency components can be reduced. With such a bandpass filter, the output of the bandpass filter is:

$$y_{BPF}(t) = BPF[y(t)]$$

$$\cong A_C \sin(\omega_C t) + A_S \sin(\omega_S t) A_C \sin(\omega_C t) \tag{13}$$

This bandpass filter output then can be demodulated either using the peak or average method to extract the transducer signal.

Conclusion

The output of a LVDT position sensor could be nonlinear. This article described how the use of a bandpass filter in the signal chain can be an effective way to deal with signal nonlinearities.

Figure 2 shows a simplified block diagram of the LVDT signal conditioner described in this article. Specifically, the block diagram shows the use of the bandpass filter in the signal chain.

Note that the PGA450-Q1 signal conditioner from Texas Instruments is designed for automotive ultrasonic park-assist sensors and already implements a bandpass filter.

References

1. Alan Oppenheim and Ronald Shafer, "Digital Signal Processing," Prentice Hall, 1975
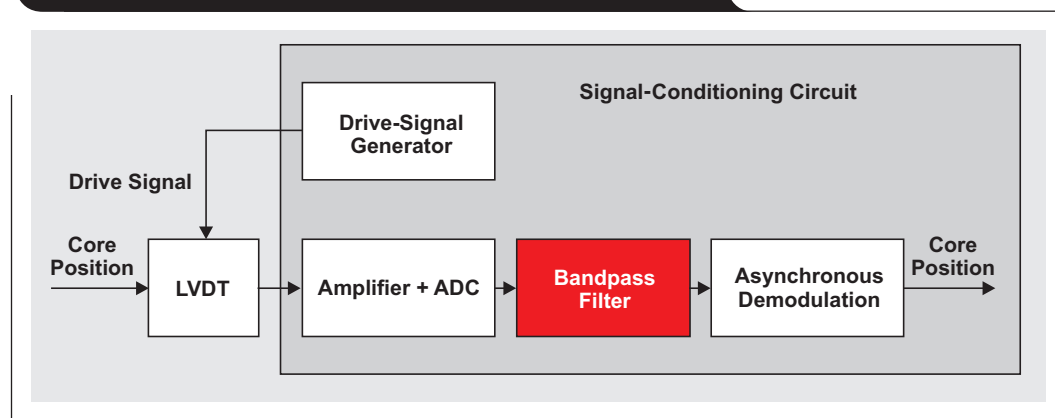
Related Web sites

www.ti.com/3q14-PGA450Q1

www.ti.com/3q14-automotive

Subscribe to the AAJ:
www.ti.com/subscribe-aaj

Figure 2: LVDT signal conditioner with bandpass filter

Decrease testing time for quality control of op amp noise

By Mohamed Tabris
Test Engineer, Precision Amplifiers

Richard Barthel
Characterization and Validation Engineer, Precision Amplifiers

Introduction

Industrial and high-precision applications require strict control over non-deterministic noise. Some testing may be required to assure system quality because the typical noise value denotes the mean value of a parameter in a population of devices, and does not guarantee that individual devices will not exceed a certain level.

Devices without guaranteed noise parameters may be rapidly tested to ensure quality. Most product data sheets for operational amplifiers (op amps) specify a typical value for 1/f noise (also known as flicker noise) for a range from 0.1 Hz to 10 Hz. Conventionally, testing devices in these situations require tens or hundreds of seconds per device, vastly increasing time-to-market and production costs.

Additionally, measuring noise density across a wide bandwidth may not be relevant in all systems or applications. To address the issue, this article uses existing theory and empirical data to explore test methodology for quickly testing for noise on any portion of the 1/f region. Furthermore, theoretical and real-world results are compared using the OPA1652 low-noise audio op amp from Texas Instruments.

Description and theory

The voltage noise-density curve of the classic op amp (Figure 1) has two regions: a frequency-independent region known as the broadband noise region; and a frequency-dependant region known as the 1/f noise region. The 1/f noise region refers to 1/f noise which, as the name suggests, exhibits a 1/f slope with respect to frequency. The 1/f noise is dominant at lower frequencies and decreases at higher frequencies. This means that it takes longer to measure than broadband noise. Low-frequency signals take longer to measure since their cycles take longer to complete in the time domain. The point at which broadband noise is equal to 1/f noise is called the corner frequency. The corner frequency for bipolar and CMOS amplifiers varies by architecture and process. Generally, bipolar amplifiers have a lower corner frequency than CMOS amplifiers.

This article presents noise as a density function, with voltage noise density having the units of $V/\sqrt{Hz}$. The voltage noise exhibited can be calculated by integrating the power spectral density between two frequencies of interest (f_1 and f_2), rather like a probability density function. The integrated voltage noise is calculated using e_n as noise spectral density:

$$V_{RMS} = \sqrt{\int_{f_1}^{f_2} \left(e_n\right)^2 df} \tag{1}$$

The combination of broadband noise and 1/f noise of an op amp (Equation 2) is obtained by taking the square root of the sum of the squares of RMS values of the broadband component and 1/f component, respectively. This is possible because broadband noise and 1/f noise are modeled as uncorrelated noise sources.

Total RMS voltage noise:

$$E_{n\_T} = \sqrt{E_{nf}^2 + E_{nBB}^2} \, , \tag{2}$$

where E_{nf} = 1/f RMS noise [V_{RMS}] and E_{nBB} = broadband RMS noise [V_{RMS}].

Figure 1. Voltage noise-density curve
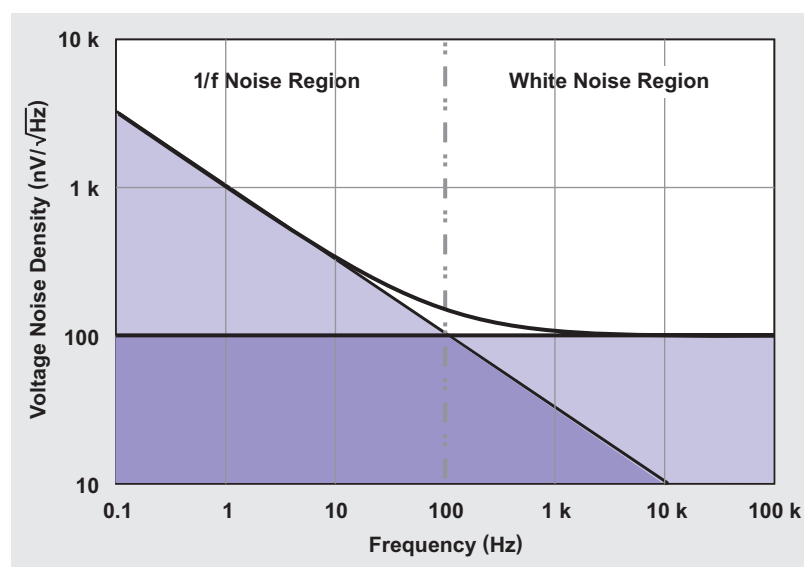
In the datasheet, the noise in the 1/f region is generally expressed in terms of peak-to-peak noise over a range of frequency, while broadband noise is expressed as a voltage noise density at a particular frequency. The units for noise spectral density are V/√Hz. The individual noise components can be calculated by using the following equations, assuming a fixed noise spectral density.

Integrated broadband noise (broadband noise constant over frequency):

$$E_{nBB} = e_{BB} \times \sqrt{BW_n} , \tag{3}$$

where e_{BB} = broadband spectral noise density [V/√Hz] and BW_n = bandwidth [Hz].

The integrated 1/f noise component:

$$E_{nf} = e_{fnorm} \times \sqrt{\ln\left(f_H / f_L\right)} , \tag{4}$$

where e_{fnorm} = normalized noise density at 1 Hz from Equation 5 [V/√Hz], f_H = upper frequency band limit [Hz], and f_L = lower frequency band limit (0.1 Hz typically) [Hz].

Normalized noise density at 1 Hz in 1/f region:

$$e_{fnorm} = e_{known} \times \frac{\sqrt{f_{known}}}{\sqrt{1 Hz}} , \tag{5}$$

where e_{known} = known voltage noise density in 1/f region [V/√Hz] and f_{known} = frequency in 1/f region where noise density is known [Hz].

The detailed calculations are shown in Reference 1 and are beyond the scope of this article.

The Problem

In noise-sensitive applications, choosing an op amp with minimal noise is critical for maintaining accuracy and precision. When selecting the op amps suitable for the application, screening may be required to remove any outliers. Testing for broadband noise occurs rapidly, since kHz cycles can be measured in just a few milliseconds. However, the same cannot be said for the 1/f noise component. Measuring the 1/f noise region can require anywhere from 0.1 seconds upwards to several minutes, depending on the bandwidth and level of averaging. This is because a cycle of the 0.1-Hz signal takes at least 10 seconds to complete. When averaging, the required time becomes even longer. Additionally, when performing a fast Fourier transform (FFT) to calculate noise density, the resolution bandwidth required may entail many hours of test time. This calls for a quick and precise way to extrapolate the 1/f noise of the op amp.

A quick and simple solution

The quickest way to test the 1/f component of the amplifier is to use Equations 4 and 5 to extrapolate. The 1/f integrated noise is proportional to the square root of the natural logarithm of the ratio of two frequencies (f_L, f_H), over which the 1/f noise is to be determined. Extending this further, one can say that a 1/f RMS noise component depends on the ratio of two frequencies: f_H and f_L. An example calculation is given by calculating 1/f RMS noise with voltage noise-density curve given (Figure 1).

To calculate 1/f RMS noise over the two ranges, 1 Hz to 10 Hz and 10 Hz to 100 Hz, assume an ideal 1/f curve with known normalized noise density e_{fnorm} at 1 Hz. Both ranges are located in the 1/f dominated portion on the noise spectral-density curve (Figure 1). This ensures a negligible error contribution from the broadband noise portion. Equation 4 is used to compare noise for the two ranges:

$$E_{nf} = e_{fnorm} \times \sqrt{\ln\left(f_N / f_L\right)}$$

$$E_{nf1} = e_{fnorm} \times \sqrt{\ln\left(10/1\right)} \,\text{and}\, E_{nf2} = e_{fnorm} \times \sqrt{\ln\left(100/10\right)}$$

$$E_{nf1} = e_{fnorm} \times \sqrt{\ln 10} \,\text{and}\, E_{nf2} = e_{fnorm} \times \sqrt{\ln 10}$$

$$E_{nf1} = e_{fnorm} \times \sqrt{\ln 10} = E_{nf2} = e_{fnorm} \times \sqrt{\ln 10}$$

Notice how the equations for E_{nf1} and E_{nf2} render the same value for 1/f RMS noise. This is because this equation is dependent on the ratio of the two frequency limits, not the frequencies themselves. There are three critical conditions for this rule of thumb to apply:

1. The 1/f curve must approximate 1/f on the power spectrum or $1/\sqrt{f}$ on the noise spectrum,
2. The area of interest must be in a 1/f-dominated region of the noise spectrum, and
3. The ratios must be the same.

Using this method, one can estimate 1/f RMS noise of an op amp from 0.1 Hz to 10 Hz by screening the op amp from 10 Hz to 1 kHz, as long as the frequencies aforementioned are in the 1/f dominated region. This change in frequency of interest improves a device's test time by a factor of 100 or more. Instead of waiting for 10 seconds for a sample to be acquired; a sample could be taken in 100 milliseconds. The most time savings are with CMOS amplifiers because the corner frequency is greater than it is for

bipolar amplifiers. The graphs in Figures 2 and 3 show that the peak-to-peak noise level of an amplifier is the same over different frequency ranges, assuming the ratio of the frequencies is equal and the measurements are in the 1/f dominant region.

Conclusion

The technique of extrapolating the 1/f noise component only holds if all frequencies are lying in the 1/f-dominated region. This technique performs with high accuracy as long as the chosen bandwidth for extrapolation is sufficiently far away from the corner frequency, because the broadband noise component is significant in this region. Additionally, the 1/f curve must approximate 1/f on the power spectrum or $1/\sqrt{f}$ on the noise spectrum. Most classical semiconductor op amps follow this rule, notable exceptions being chopper or auto-zero amplifiers that do not have a 1/f noise region. One example is the low-noise, zero-drift OPA2188.

Acknowledgments

References

1. Art Kay, "Analysis and measurement of intrinsic noise in op amp circuits," AnalogZone, 2006. Available: **www.ti.com/3q14-slyy061**
2. Art Kay, "Operational amplifier noise: Techniques and tips for analyzing and reducing noise (1st ed.)," Elsevier Inc., January 27, 2012
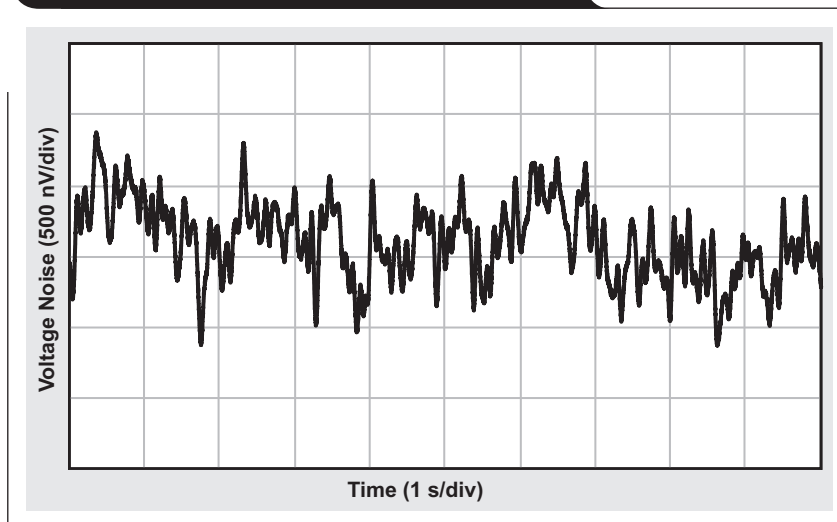
Related Web sites

www.ti.com/3q14-OPA1652

www.ti.com/3q14-OPA2188

Subscribe to the AAJ:
www.ti.com/subscribe-aaj

Figure 2. Voltage noise from 0.1 Hz to 10 Hz

Figure 3. Voltage noise from 1 Hz to 100 Hz
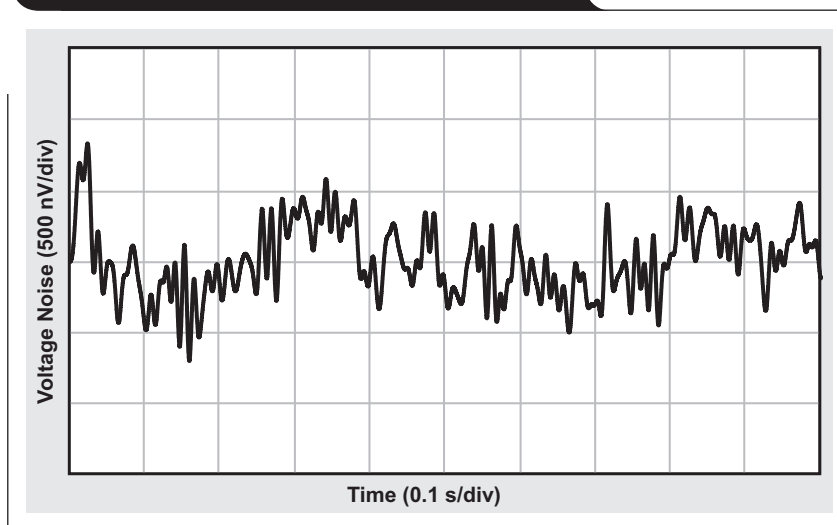
Design tips for an efficient non-inverting buck-boost converter

By Haifeng Fan
Systems Engineer, Power Management

Introduction

Buck-boost (step-down and step-up) converters are widely used in industrial personal computers (IPCs), point-of-sale (POS) systems, and automotive start-stop systems. In these applications, the input voltage could be either higher or lower than the desired output voltage. A basic inverting buck-boost converter has a negative output voltage with respect to ground. The single-end primary inductor converter (SEPIC), Zeta converter, and two-switch buck-boost converters have positive or non-inverting outputs. However, compared with a basic inverting buck-boost converter, all three non-inverting topologies have additional power components and reduced efficiency. This article presents operational principles, current stress and power-loss analysis of these buck-boost converters, and presents design criteria for an efficient non-inverting buck-boost converter.

Inverting buck-boost converter

Figure 1 shows the schematic of a basic inverting buck-boost converter, along with the typical voltage and current waveforms in continuous conduction mode (CCM). In addition to input and output capacitors, the power stage consists of a power metal-oxide semiconductor field-effect transistor (MOSFET), a diode, and an inductor. When the MOSFET (Q1) is ON, the voltage across the inductor (L1) is V_{IN}, and the inductor current ramps up at a rate that is proportional to V_{IN}. This results in accumulating energy in the inductor. While Q1 is ON, the output capacitor supplies the entire load current. When the Q1 is OFF, the diode (D1) is forward-biased and the inductor current ramps down at a rate proportional to V_{OUT}. While Q1 is OFF, energy is transferred from the inductor to the output load and capacitor.

The voltage conversion ratio of an inverting buck-boost in CCM can be expressed as:
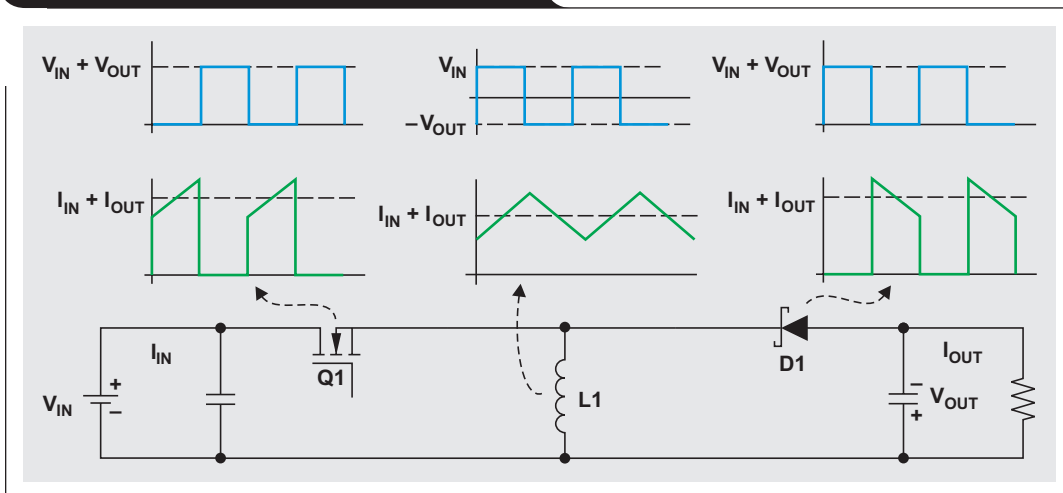
$$M = \frac{V_{OUT}}{V_{IN}} = -\frac{D}{1-D},\tag{1}$$

where D is the duty cycle of Q1 and is always in a range of 0 to 1. Equation 1 indicates that the magnitude of output voltage could be either higher (when D > 0.5) or lower (when D < 0.5) than the input voltage. However, the output voltage always has an inverse polarity relative to the input.

Conventional non-inverting buck-boost converters

The inverting buck-boost converter does not serve the needs of applications where a positive output voltage is required. The SEPIC, Zeta, and two-switch buck-boost converter are three popular non-inverting buck-boost topologies. The Zeta converter, also called inverse SEPIC, is similar to SEPIC, but less attractive than SEPIC since it requires a high-side driver that increases the circuit complexity.

Figure 1. Inverting buck-boost converter

A SEPIC converter and its ideal waveforms in CCM are shown in Figure 2. The voltage conversion ratio of a SEPIC converter is:

$$M = \frac{V_{OUT}}{V_{IN}} = \frac{D}{1-D}. \qquad (2)$$

Equation 2 indicates a positive output voltage and the buck-boost capability.
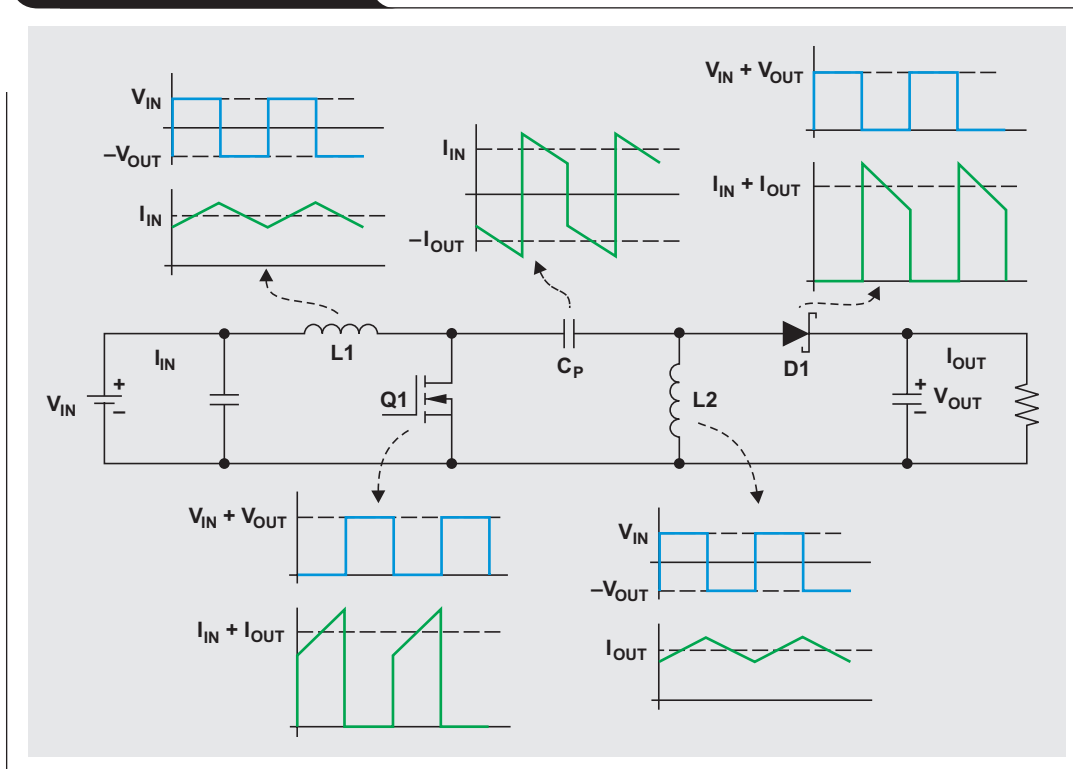
Like an inverting buck-boost converter, a SEPIC converter has a single MOSFET (Q1) and a single diode (D1). The MOSFET and diode in a SEPIC converter have voltage and current requirements similar to their counterparts in an inverting buck-boost converter. As such, the power losses of the MOSFET and diode are similar. On the other hand, a SEPIC converter has an additional inductor (L2) and an additional ac-coupling capacitor (C$_P$).

In a SEPIC converter, the average inductor current of L1 equals the input current (I$_{IN}$), whereas the average

inductor current of L2 equals the output current (I$_{OUT}$). In contrast, the single inductor in an inverting buck-boost converter has an average current of I$_{IN}$ + I$_{OUT}$. The coupling capacitor sees significant root-mean-square (RMS) current relative to both input current and output current, which generates extra power loss and reduces the converter's overall efficiency.

To reduce power loss, ceramic capacitors with low equivalent series resistance (ESR) are desired, which usually leads to higher cost. The additional inductor of a SEPIC converter, coupled with the extra coupling capacitor, increases printed circuit board (PCB) size and total solution cost. A coupled inductor can be used to replace two separate inductors to reduce PCB size. However, the selection of off-the-shelf coupled inductors are limited when compared to separate inductors. Sometimes a custom design will be required, which increases cost and lead time.

Figure 2. SEPIC converter

A conventional two-switch buck-boost converter uses a single inductor (Figure 3). However, it has an additional MOSFET (Q2) and an additional diode (D2) compared to an inverting buck-boost converter. By turning Q1 and Q2 ON and OFF simultaneously, the converter operates in buck-boost mode, and the voltage conversion ratio also complies with Equation 2. This confirms that the two-switch buck-boost converter performs a non-inverting conversion. The ideal waveforms of a two-switch buck-boost converter operating in buck-boost mode and CCM are shown in Figure 3. Q1 and D1 both see a voltage stress of V_{IN}, while Q2 and D2 both see a voltage stress of V_{OUT}. Q1, Q2, D1, D2, and L1 all see a current stress of $I_{IN} + I_{OUT}$ with inductor ripple current neglected. The relatively large

number of power devices and high-current stress in buck-boost mode prevent the converter from being very efficient.

Operating-mode optimization of a two-switch buck-boost converter

The two-switch buck-boost converter is a cascaded combination of a buck converter followed by a boost converter. Besides the aforementioned buck-boost mode, wherein Q1 and Q2 have identical gate-control signals, the two-switch buck-boost converter also can operate in either buck or boost mode. By operating the converter in buck mode when V_{IN} is higher than V_{OUT}, and in boost mode when V_{IN} is lower than V_{OUT}, the buck-boost function is then realized.

Figure 3. A two-switch buck-boost converter in buck-boost mode of operation
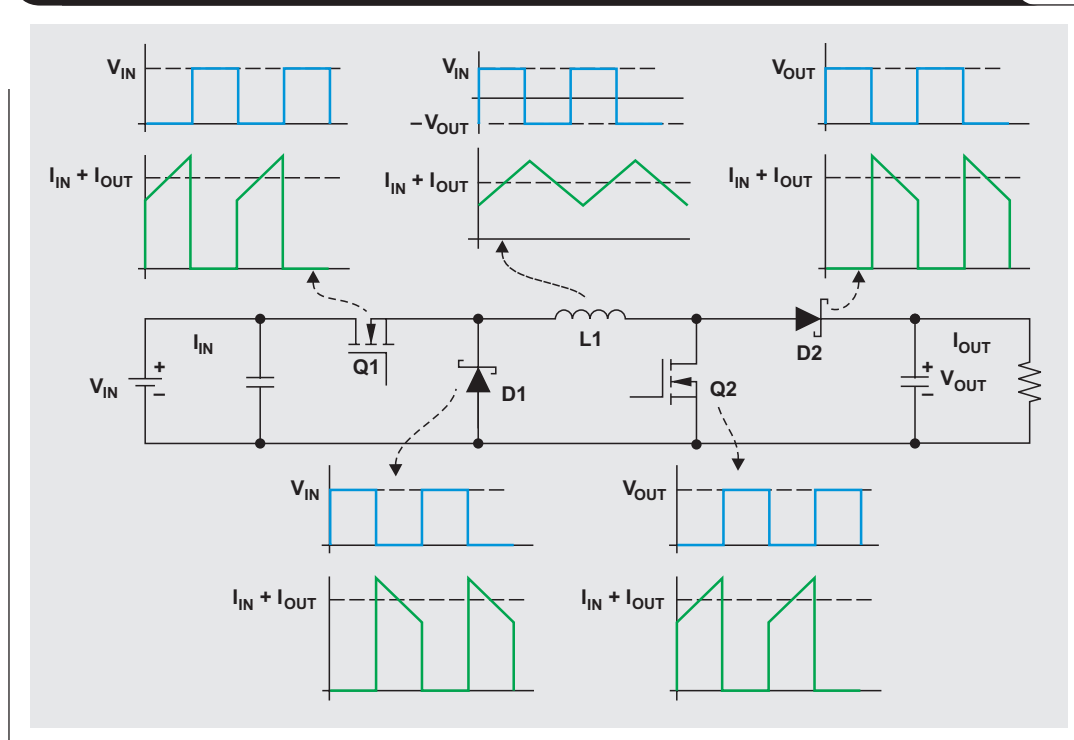
In buck mode, Q2 is controlled to be always OFF, and output voltage is regulated by controlling Q1 as in a typical buck converter. The equivalent circuit in buck mode and corresponding ideal waveforms in CCM are shown in Figure 4. The voltage conversion ratio is the same as that of a typical buck converter:

$$M = \frac{V_{OUT}}{V_{IN}} = D, \qquad (3)$$

where D is the duty cycle of Q1. In buck mode, the output voltage is always lower than the input voltage since D is always less than one.

Higher efficiency is possible in buck mode compared to the buck-boost mode for three reasons. First of all, Q2 is always OFF in buck mode, which means there is no power dissipated in it. Second, Q1, D1, and L1 see a lower current stress of only I_{OUT} in buck mode compared to $I_{IN} + I_{OUT}$ in buck-boost mode, which potentially reduces power loss. Third, although conduction loss of D2 stays the same,

the reverse recovery loss is eliminated in the buck mode because D2 always conducts.

By keeping Q1 always ON, D1 is reverse biased and stays OFF, and the two-switch buck-boost converter then operates in boost mode. Similar to the typical boost converter, the output voltage is regulated by controlling Q2. The equivalent circuit in boost mode and corresponding ideal waveforms in CCM are shown in Figure 5. The voltage conversion ratio is the same as that of a typical boost converter:

$$M = \frac{V_{OUT}}{V_{IN}} = \frac{1}{1-D}, \qquad (4)$$

where D is the duty cycle of Q2. In boost mode, the output voltage is always greater than the input voltage because D is always greater than zero. Similarly, higher efficiency could be achieved in boost mode than in buck-boost mode due to fewer operating power devices and lower current stress.

Figure 4. Buck-mode operation of the two-switch buck-boost converter
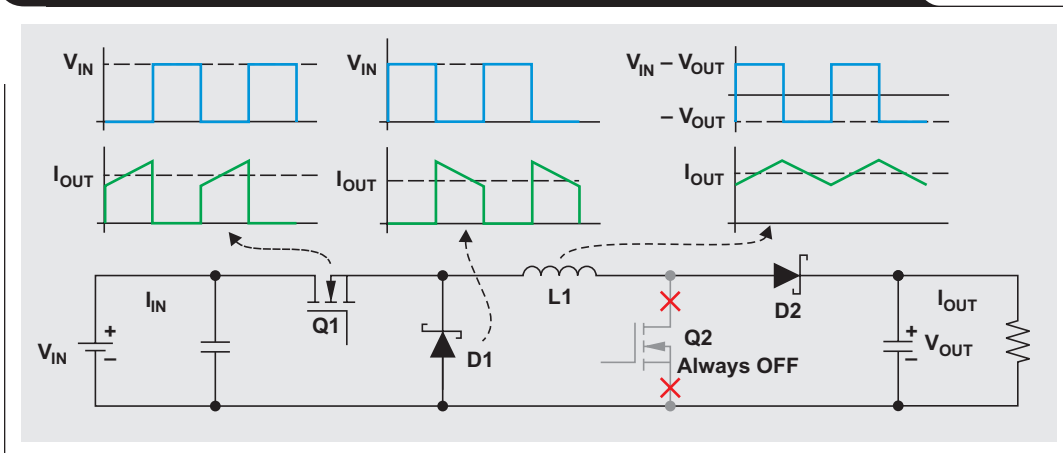
Figure 5. Boost-mode operation of the two-switch buck-boost converter
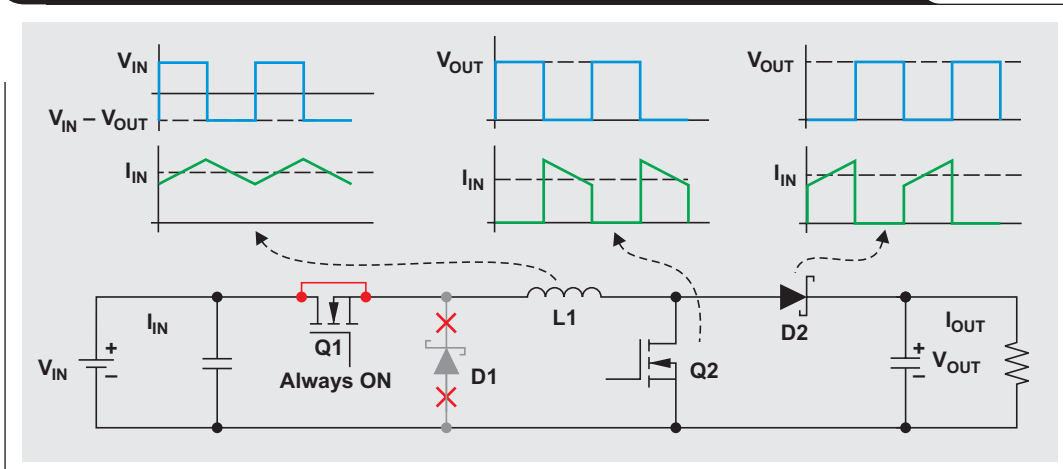
Implementation of an efficient two-switch buck-boost converter

The two-switch buck-boost converter can function in buck-boost, buck or boost modes of operation. Various combinations of operating modes can be used to accomplish both a step-up and step-down function. Appropriate control circuitry is required to ensure the desired modes of operation. Table 1 summarizes a comparison between four different combinations of operating modes. The buck-boost mode alone features the simplest control, but has low efficiency for both step-up and step-down conversion over the V_{IN} range.

**Table 1. Comparison of operating modes**

OPERATION MODES	CONTROL COMPLEXITY	EFFICIENCY ($V_{IN} > V_{OUT}$)	EFFICIENCY ($V_{IN} < V_{OUT}$)
Buck-boost	Simple	Low	Low
Buck and buck-boost	Moderate	High	Low
Buck-boost and boost	Moderate	Low	High
Buck, buck-boost, and boost	Complicated	High	High

The combination of buck, buck-boost and boost modes has the potential to achieve high efficiency over the V_{IN} range. However, its control is very complicated due to multiple modes of operation and the resulting transitions between different modes. In many applications, the input voltage usually drops below output for only a short period of time. In such applications, the efficiency of step-up conversion is not as critical as step-down conversion. As such, the combination of buck and buck-boost modes is a good trade-off between control complexity and efficiency.

Figure 6 shows a practical implementation of a two-switch buck-boost converter that uses the LM5118 dual-mode controller from Texas Instruments. This converter acts as a buck converter when the input voltage is above the output voltage. As the input voltage decreases and falls below the output voltage, it transits to buck-boost mode. There is a short gradual transition region between buck mode and buck-boost mode to eliminate disturbances at the output during transitions.

In this example, the nominal output voltage is 12 V. When V_{IN} is above 15.5 V, the converter operates in buck mode. When V_{IN} falls below 13.2 V, the converter operates

Figure 6. Two-switch buck-boost converter features buck and buck-boost operating modes
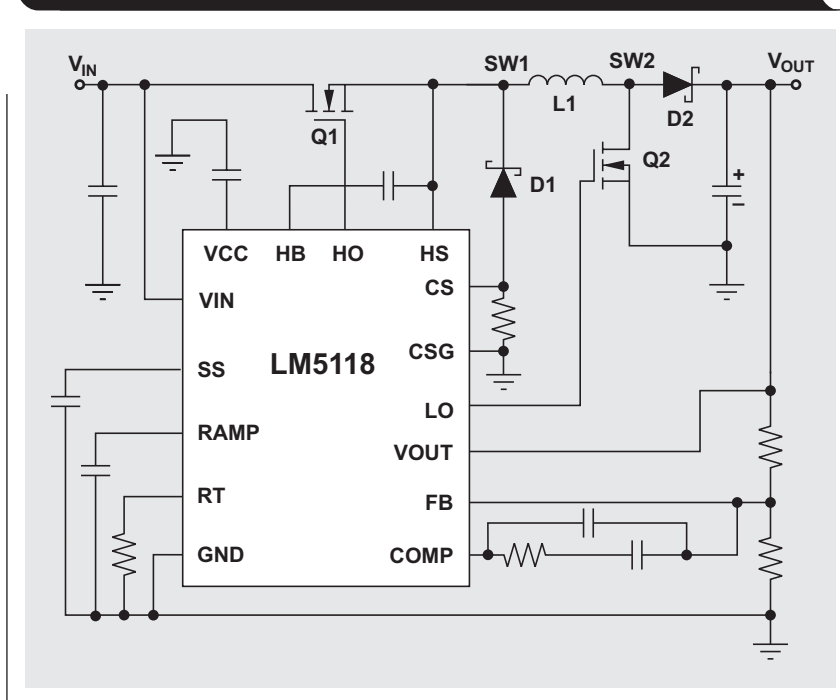
in buck-boost mode. When V_{IN} is between 15.5 V and 13.2 V, the converter operates in the transition mode. Figure 7 shows voltage waveforms of switch node 1 (SW1) and switch node 2 (SW2). In buck mode (V_{IN} = 24 V), SW2 voltage stays constant which suggests that Q2 is kept OFF. In contrast, Q2 as well as Q1 are switching in buck-boost mode (V_{IN} = 9 V). Figure 8 shows the efficiency with respect to input voltage at 3 A of load current. The improved efficiency for step-down conversion is achieved by operating the converter in buck mode.

Conclusion

SEPIC, Zeta, and two-switch buck-boost converters are three popular non-inverting buck-boost topologies that provide a positive output as well as a step-up/down function. When operating in the buck-boost mode, all three converters can experience high-current stress and high-conduction loss. However, by operating the two-switch buck-boost converter in either buck mode or boost mode, the current stress can be reduced and the efficiency can be improved.

References

1. "AN-1157 Positive to Negative Buck-Boost Converter Using LM267X SIMPLE SWITCHER® Regulators," Application Report, Texas Instruments, April 2013. Available: **www.ti.com/3q14-SNVA022**

Related Web sites

www.ti.com/3q14-LM5118

www.ti.com/3q14-LM5022

Subscribe to the AAJ:
www.ti.com/subscribe-aaj

Figure 7. Voltage waveforms at switch nodes

(a.) Buck mode when V_{IN} = 24 V

(b.) Buck-boost mode when V_{IN} = 9 V
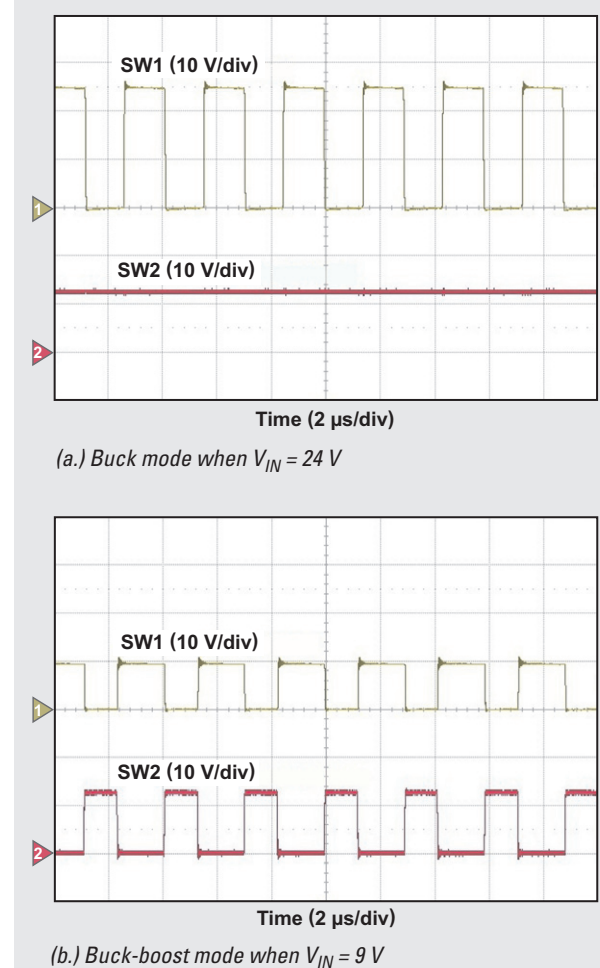
Figure 8. Efficiency with respect to the input voltage
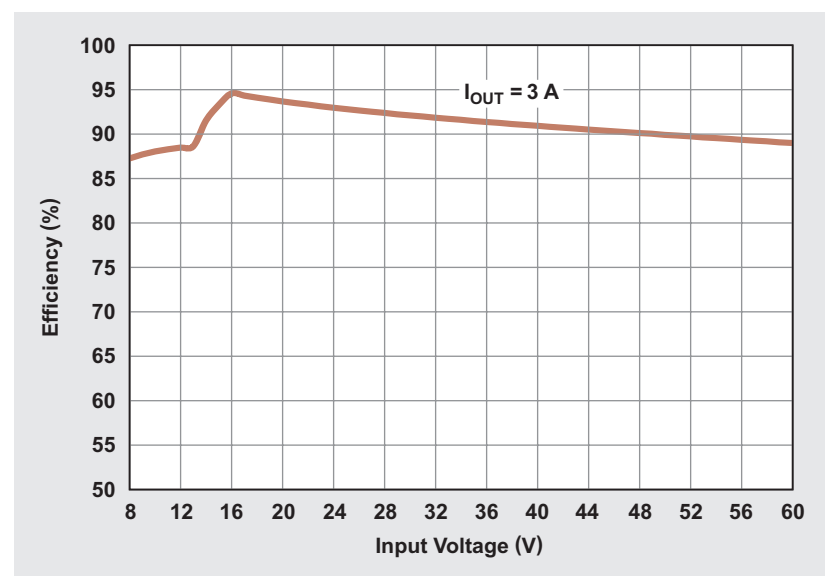
AC cycle skipping improves PFC light-load efficiency

By Bosheng Sun
Systems Engineer

For power supplies with an input power of 75 watts or greater, power factor correction (PFC) is usually required. It forces the input current to follow the input voltage, so that any electrical load appears like a resistor to the voltage source that powers it. This is essential for many server, telecommunications and industrial applications, where energy efficiency and power quality have become more and more strict. The most important criteria to judge PFC performance is efficiency, total harmonic distortion (THD), and power factor (PF). With the help of new semiconductor devices and new control methods, the modern PFC circuit has achieved very good performance at middle and heavy loads. However, during light-load conditions, the efficiency, THD and PF deteriorate significantly.

A typical PFC efficiency curve is shown in Figure 1. Notice how the efficiency gets lower and lower at light loads. This is because the switching loss, driving loss, and reverse-recovery loss of semiconductor components become dominant at light loads. Meanwhile, a PFC may transition from continuous-conduction mode (CCM) to discontinuous-conduction mode (DCM), which causes

the converter dynamics to change abruptly and the current-loop bandwidth to reduce significantly. The small current-feedback signal also makes control very difficult. As a result, the THD of the current waveform increases (Figure 2).

This article provides a novel method to increase efficiency and reduce THD when the PFC enters the light-load condition. In this method, when the load is reduced to less than a predefined threshold, the PFC enters a special burst-mode. In this mode, depending on the load, one or more AC cycles are skipped by the PFC. In other words, the PFC turns off for one or more AC cycles, and turns back on for the next AC cycle. The turn-on/turn-off instance is at the AC zero-crossing, such that the whole AC cycle is skipped. Moreover, since PFC turn-on/turn-off occurs when the current equals zero, less stress and electromagnetic interference (EMI) noise are generated. This is different than the traditional PWM pulse-skipping burst-mode, where the PWM pulses are skipped randomly.

The number of AC cycles to be skipped is inversely proportional to the load. If the load continues to decrease below the threshold, additional AC cycles will be skipped.

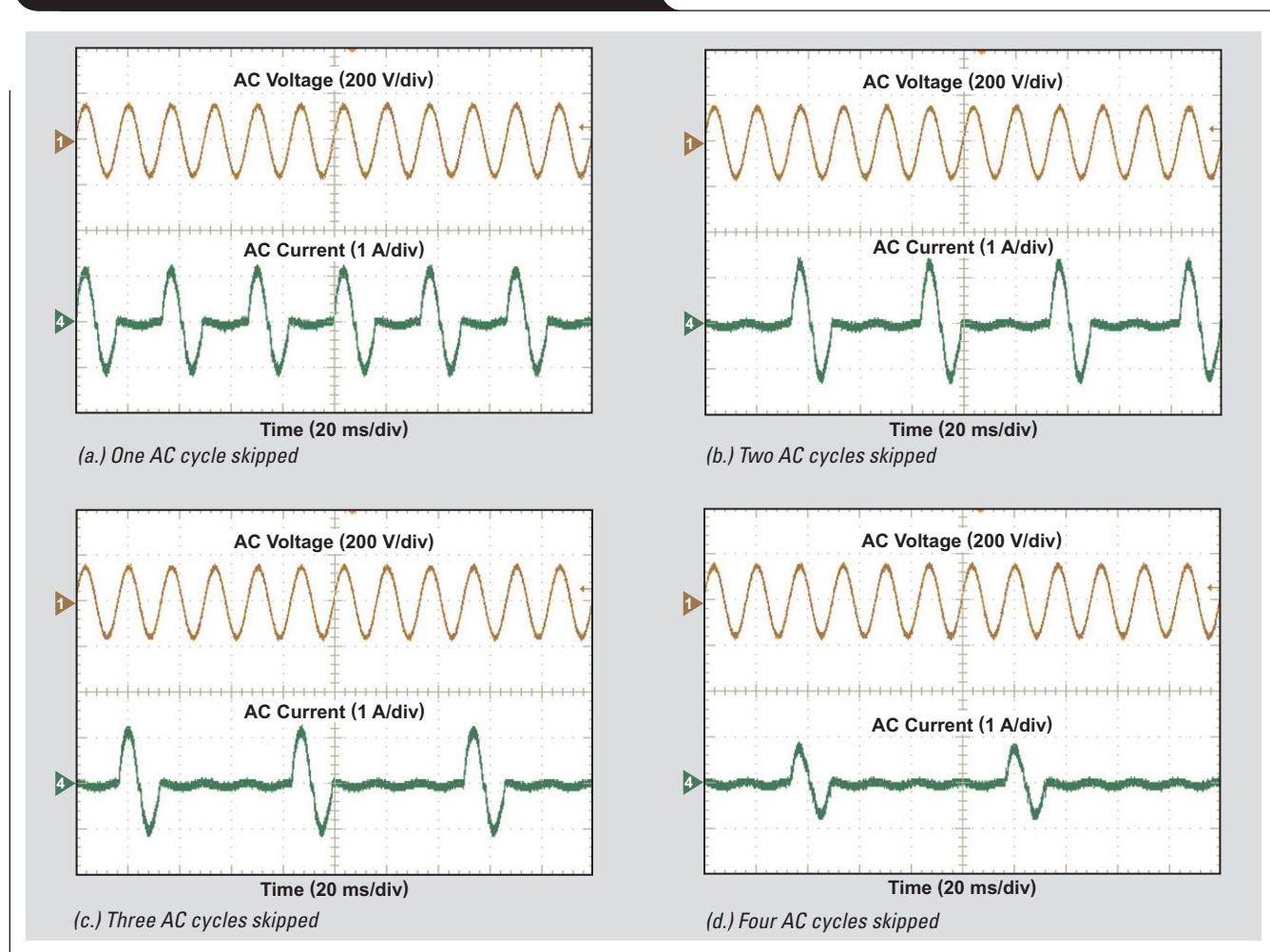**Figure 1. Example of a typical PFC efficiency curve**
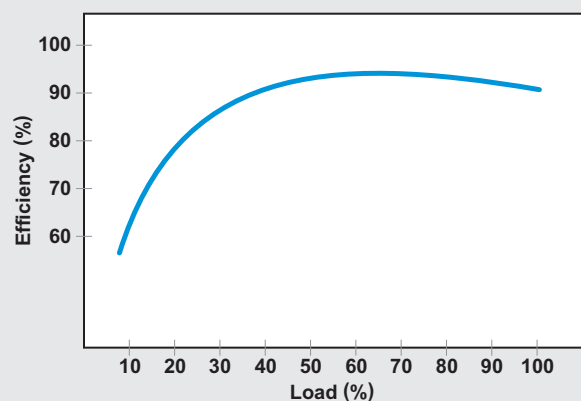
Figure 2. Example of a typical PFC THD curve
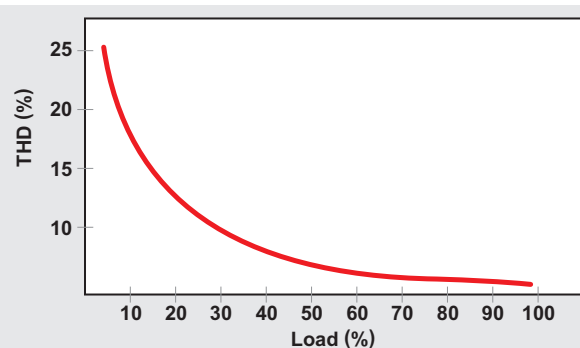
A look-up table can be generated with the load versus the number of cycles to be skipped. This table will show the maximum number of AC cycles can be skipped while maintaining the output voltage ripple within a specified range. Figure 3 shows four different AC cycles that are skipped at different loads.

Once the PFC turns off, the switching loss, driving loss, and reverse-recovery loss are all reduced to zero, and the power loss is just the PFC stand-by power. Since the current is zero, THD is zero. When the PFC turns on, it delivers more than the power required by a light load because it needs to compensate for the turn-off period. Because

Figure 3. AC cycles being skipped at different loads

(a.) One AC cycle skipped

(b.) Two AC cycles skipped

(c.) Three AC cycles skipped

(d.) Four AC cycles skipped

the PFC now operates at middle load or completely shuts off to skip AC cycles, the light-load efficiency is increased and THD is reduced. Figures 4 and 5 show the efficiency and THD improvements with this special burst-mode.

Note that when PFC turns off to skip AC cycles, both the current loop and voltage loop need to be frozen. Otherwise, the integrators in these loops build up to generate a big PWM pulse when the PFC turns back on, which causes a large current spike.

To determine whether or not the PFC enters the light-load condition, the load information needs to be monitored. Normally there is no current sensor at the PFC output, so to directly measuring output load is not

feasible. However, the PFC voltage-loop output is proportional to the load when V_{IN} is fixed. Therefore, the loop output can be used as a rough indicator to determine whether or not the PFC is operating with a light load.

If there is a requirement for the precise number of AC cycles to be skipped in order to maintain the output voltage ripple within a specified range, accurate load information is required. Since there is a current shunt measuring input current for PFC current-loop regulation, the input power of a PFC can be measured. The input current and voltage can be monitored by analog-to-digital converters (ADCs), and then used to calculate the real input power. This accurate input-power information can be used to
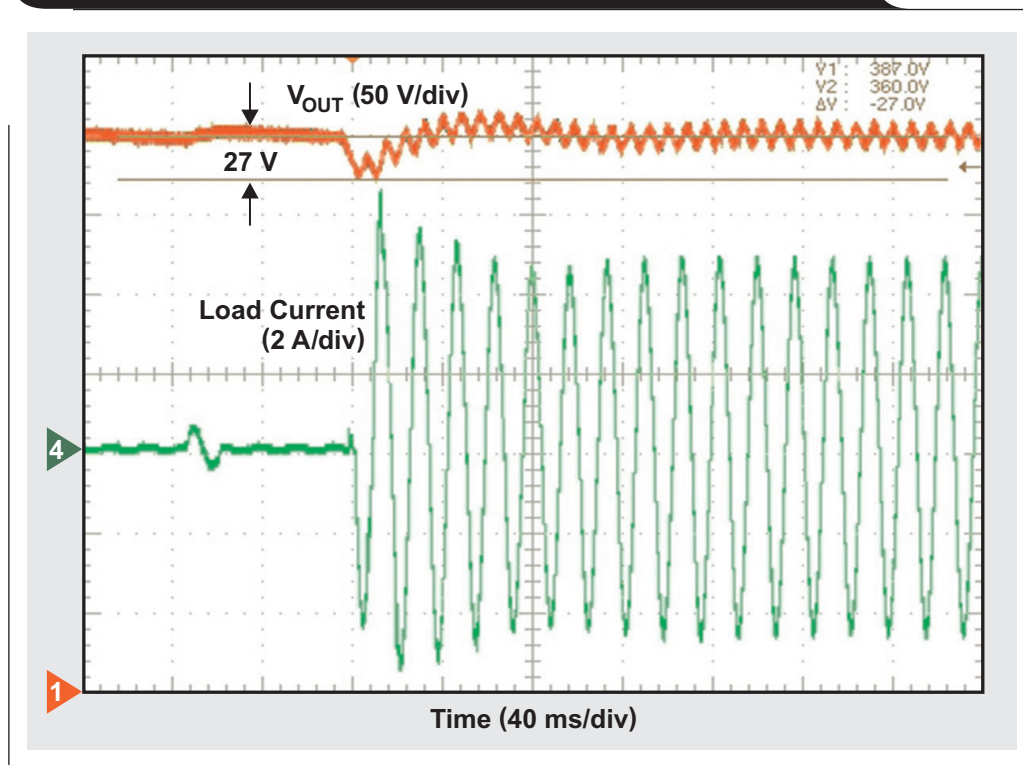
Figure 4: Efficiency comparison
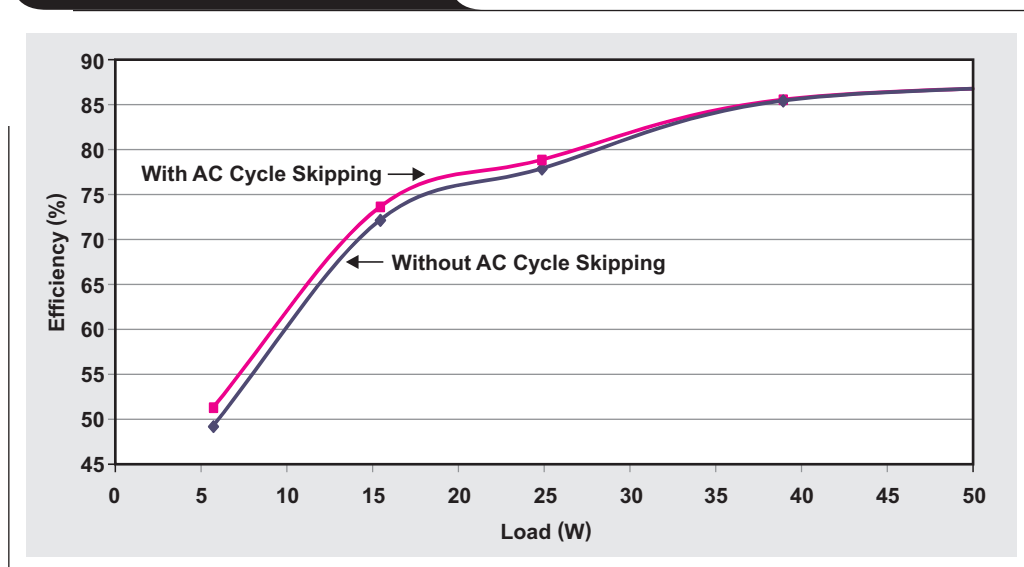
Figure 5: THD comparison
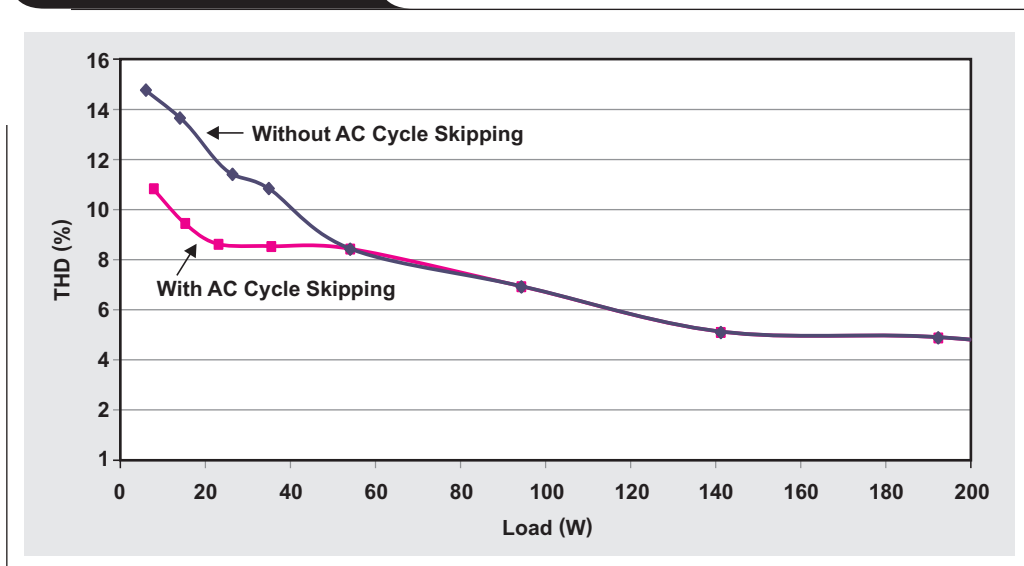
Figure 6. Load transient from zero to 100% during AC cycle skipping

precisely adjust the number of AC cycles to be skipped. There is no need for any extra hardware. For details of accurate PFC input-power measurement, please see Reference 1.

A big concern of this approach is the output voltage drop during a load transient. Assuming a load step-up occurs when the PFC is off, V_{OUT} may drop too much. To address this issue, V_{OUT} is compared with a predefined threshold through a comparator. Once V_{OUT} is below this threshold, the PFC will immediately exit the burst mode, AC cycle skipping is disabled, and the PFC returns to normal operation. It will handle transient response as if there is no special burst mode. Figure 6 shows the effects of a load transient from 0 to 100% during AC cycle skipping. Note that the V_{OUT} drop during the transient is only 27 V, which is very normal for a 360-W PFC.

Conclusion

A novel PFC burst mode allows one or more AC cycles to be skipped when a PFC operates with a light load. As a result, both efficiency and THD are improved. Moreover,

since the PFC turns on/off at AC zero-crossing, circuit stress and EMI noise are reduced. The number of AC cycles to be skipped can be precisely adjusted based on load to maximize performance and maintain the output voltage ripple within a specified range. If a load transient occurs when the PFC is off, the burst mode is disabled immediately and the PFC handles the effects of the load transient normally. Finally, the implementation is easy with a digital controller, and no extra hardware is needed.

References

1. Bosheng Sun, "Low-cost solution for measuring input power and RMS current," Analog Applications Journal, Texas Instruments, 4Q 2013. Available: **www.ti.com/3q14-SLYT545**

Related Web sites

www.ti.com/3q14-UCD3138

Subscribe to the AAJ: **www.ti.com/subscribe-aaj**

TI Worldwide Technical Support

Internet

TI Semiconductor Product Information Center Home Page
support.ti.com

TI E2E™ Community Home Page
e2e.ti.com

Product Information Centers

Americas	Phone	+1(512) 434-1560
Brazil	Phone	0800-891-2616
Mexico	Phone	0800-670-7544
	Fax	+1(972) 927-6377
	Internet/Email	support.ti.com/sc/pic/americas.htm

Europe, Middle East, and Africa

Phone
European Free Call	00800-ASK-TEXAS (00800 275 83927)
International	+49 (0) 8161 80 2121
Russian Support	+7 (4) 95 98 10 701

Note: The European Free Call (Toll Free) number is not active in all countries. If you have technical difficulty calling the free call number, please use the international number above.

Fax	+(49) (0) 8161 80 2045
Internet	www.ti.com/asktexas
Direct Email	asktexas@ti.com

Japan

Fax	International	+81-3-3344-5317
	Domestic	0120-81-0036
Internet/Email	International	support.ti.com/sc/pic/japan.htm
	Domestic	www.tij.co.jp/pic

Asia

Phone   Toll-Free Number
Note: Toll-free numbers may not support mobile and IP phones.

Australia	1-800-999-084
China	800-820-8682
Hong Kong	800-96-5941
India	000-800-100-8888
Indonesia	001-803-8861-1006
Korea	080-551-2804
Malaysia	1-800-80-3973
New Zealand	0800-446-934
Philippines	1-800-765-7404
Singapore	800-886-1028
Taiwan	0800-006800
Thailand	001-800-886-0010
International	+86-21-23073444
Fax	+86-21-23073686
Email	tiasia@ti.com or ti-china@ti.com
Internet	support.ti.com/sc/pic/asia.htm

Important Notice: The products and services of Texas Instruments Incorporated and its subsidiaries described herein are sold subject to TI's standard terms and conditions of sale. Customers are advised to obtain the most current and complete information about TI products and services before placing orders. TI assumes no liability for applications assistance, customer's applications or product designs, software performance, or infringement of patents. The publication of information regarding any other company's products or services does not constitute TI's approval, warranty or endorsement thereof.

A021014

E2E and OMAP are trademarks and DLP and SIMPLE SWITCHER are registered trademarks of Texas Instruments. All other trademarks are the property of their respective owners.

SLYT586

IMPORTANT NOTICE

Texas Instruments Incorporated and its subsidiaries (TI) reserve the right to make corrections, enhancements, improvements and other changes to its semiconductor products and services per JESD46, latest issue, and to discontinue any product or service per JESD48, latest issue. Buyers should obtain the latest relevant information before placing orders and should verify that such information is current and complete. All semiconductor products (also referred to herein as "components") are sold subject to TI's terms and conditions of sale supplied at the time of order acknowledgment.

TI warrants performance of its components to the specifications applicable at the time of sale, in accordance with the warranty in TI's terms and conditions of sale of semiconductor products. Testing and other quality control techniques are used to the extent TI deems necessary to support this warranty. Except where mandated by applicable law, testing of all parameters of each component is not necessarily performed.

TI assumes no liability for applications assistance or the design of Buyers' products. Buyers are responsible for their products and applications using TI components. To minimize the risks associated with Buyers' products and applications, Buyers should provide adequate design and operating safeguards.

TI does not warrant or represent that any license, either express or implied, is granted under any patent right, copyright, mask work right, or other intellectual property right relating to any combination, machine, or process in which TI components or services are used. Information published by TI regarding third-party products or services does not constitute a license to use such products or services or a warranty or endorsement thereof. Use of such information may require a license from a third party under the patents or other intellectual property of the third party, or a license from TI under the patents or other intellectual property of TI.

Reproduction of significant portions of TI information in TI data books or data sheets is permissible only if reproduction is without alteration and is accompanied by all associated warranties, conditions, limitations, and notices. TI is not responsible or liable for such altered documentation. Information of third parties may be subject to additional restrictions.

Resale of TI components or services with statements different from or beyond the parameters stated by TI for that component or service voids all express and any implied warranties for the associated TI component or service and is an unfair and deceptive business practice. TI is not responsible or liable for any such statements.

Buyer acknowledges and agrees that it is solely responsible for compliance with all legal, regulatory and safety-related requirements concerning its products, and any use of TI components in its applications, notwithstanding any applications-related information or support that may be provided by TI. Buyer represents and agrees that it has all the necessary expertise to create and implement safeguards which anticipate dangerous consequences of failures, monitor failures and their consequences, lessen the likelihood of failures that might cause harm and take appropriate remedial actions. Buyer will fully indemnify TI and its representatives against any damages arising out of the use of any TI components in safety-critical applications.

In some cases, TI components may be promoted specifically to facilitate safety-related applications. With such components, TI's goal is to help enable customers to design and create their own end-product solutions that meet applicable functional safety standards and requirements. Nonetheless, such components are subject to these terms.

No TI components are authorized for use in FDA Class III (or similar life-critical medical equipment) unless authorized officers of the parties have executed a special agreement specifically governing such use.

Only those TI components which TI has specifically designated as military grade or "enhanced plastic" are designed and intended for use in military/aerospace applications or environments. Buyer acknowledges and agrees that any military or aerospace use of TI components which have *not* been so designated is solely at the Buyer's risk, and that Buyer is solely responsible for compliance with all legal and regulatory requirements in connection with such use.

TI has specifically designated certain components as meeting ISO/TS16949 requirements, mainly for automotive use. In any case of use of non-designated products, TI will not be responsible for any failure to meet ISO/TS16949.

Products		Applications	
Audio	www.ti.com/audio	Automotive and Transportation	www.ti.com/automotive
Amplifiers	amplifier.ti.com	Communications and Telecom	www.ti.com/communications
Data Converters	dataconverter.ti.com	Computers and Peripherals	www.ti.com/computers
DLP® Products	www.dlp.com	Consumer Electronics	www.ti.com/consumer-apps
DSP	dsp.ti.com	Energy and Lighting	www.ti.com/energy
Clocks and Timers	www.ti.com/clocks	Industrial	www.ti.com/industrial
Interface	interface.ti.com	Medical	www.ti.com/medical
Logic	logic.ti.com	Security	www.ti.com/security
Power Mgmt	power.ti.com	Space, Avionics and Defense	www.ti.com/space-avionics-defense
Microcontrollers	microcontroller.ti.com	Video and Imaging	www.ti.com/video
RFID	www.ti-rfid.com		
OMAP Applications Processors	www.ti.com/omap	**TI E2E Community**	e2e.ti.com
Wireless Connectivity	www.ti.com/wirelessconnectivity		